Phase shift analysis of 0–30 MeV pp scattering data

J. R. Bergervoet, P. C. van Campen, W. A. van der Sanden, and J. J. de Swart
Institute for Theoretical Physics, University of Nijmegen, Nijmegen, The Netherlands
(Received 27 April 1987)

A multienergy phase shift analysis of all published proton-proton (pp) scattering data in the energy range $T_{lab} \leq 30$ MeV is presented. In the description of all partial waves the well-known long-range interaction is included: the improved Coulomb, the vacuum polarization, and the one-pion-exchange potential. In the lower partial waves the energy-dependent analysis uses a P-matrix parametrization for the short-range interaction. Special attention is paid to the electric interaction, the definition of the phase shifts, and the selection of the data. The fit to the final data set comprising 360 scattering observables results in $\chi^2/N_{df}=1.0$, where N_{df} is the number of degrees of freedom. The $pp\pi^0$ coupling constant is determined to be $g^2_{pp\pi^0}/4\pi=14.5\pm1.2$, but there are several indications for a lower value. The optimum value for the P-matrix radius $b\approx1.4$ fm is satisfying. Single-energy phase shifts with second derivative matrices, and effective range parameters are given.

I. INTRODUCTION

An analysis is presented of all proton-proton (pp) scattering data at laboratory kinetic energies $T_{lab} \leq 30$ MeV. Since the latest analysis of this low-energy region by Naisse[1,2] in 1977, the world set of pp scattering data has grown considerably,[3–10] mainly below 10 MeV.

On the theoretical side, improvements over earlier low-energy analyses[2,11,12] have been made by inclusion of an improved Coulomb potential[13,14] and an explicit treatment of pion-exchange effects. Our P-matrix parametrization of the lower partial waves was an important improvement especially for the $^1S_0$ partial wave. All parametrized partial waves, the S, P, and D waves, are treated in the same manner. In an analysis the partial waves with higher angular momentum have to be taken from theory. In these partial waves we used the phase shifts due to vacuum polarization (VP) and one-pion exchange (OPE), computed in Coulomb-distorted-wave Born approximation (CDWBA).

In order to get a good fit to the data in this low-energy region, one has to take into account VP, OPE, and the relativistic Coulomb parameter η'. The use of the CDWBA instead of the plane-wave Born approximation (BA) in the higher partial waves, and the inclusion of the full improved Coulomb potential instead of only keeping the η' term are less important. They give no significant improvement of the fit, but they do influence the precise values that are found for the phase shifts and the pion-nucleon coupling constant.

In the past the most widely used parametrizations for the phase shifts at low energies have been effective range expansions.[15,16,2,17,18] At those energies most of the scattering happens in the $^1S_0$ state. At 10 MeV, for instance, more than 99% of the differential cross section is produced by the nuclear interaction in the $^1S_0$ partial wave and the electromagnetic interaction. Heller[19] derived for the $^1S_0$ an effective range function, in which Coulomb and VP were included. If additional electromagnetic effects are neglected, this effective range function will have as its most nearby singularity a cut due to OPE, starting at $T_{lab}=-9.7$ MeV in the complex energy plane. Because this is rather close to the physical energy region, several analyses[11,2] used the Cini-Fubini-Stanghellini (CFS)[20,21] approximation, which tries to take this nearby singularity approximately into account. It has been shown[17,14] in a potential model by comparing the CFS approximation with the calculated effective range function, that the CFS approximation is totally unsuitable for a proper description of the $^1S_0$ partial wave.

Recently, an analysis up to 3 MeV has been done[17] in which the $^1S_0$ phase shift was parametrized as a function of the energy using a pion-modified effective range formalism. This approach gives practically identical results as our P-matrix formalism, even for the entire 0–30 MeV range. The major drawback of modified effective range expansions is the large effort necessary to compute the modified effective range function with sufficient accuracy. This problem arises from the singular behavior near the origin of the long-range (Coulomb, VP) potentials. The incentive of the modified effective range formalism was only to remove the singularities near $T_{lab}=0$ of the effective range function, caused by the tail of the long-range potentials. Since the short-range interaction is parametrized anyway, one can see that the accuracy problem of the modified effective range method is an artificial one, arising from a too-detailed treatment of the short-range part of the long-range potential. For higher angular momenta the situation becomes even worse, due to the appearance of the centrifugal barrier.

In other analyses[2,12] the interaction in the $^1S_0$ state was parametrized by means of a parametrized potential. The advantage of this method is that the electromagnetic and OPE interactions are easily included in the correct way, thereby fixing the tail of the potential. But it appears that very different forms of the potential in the inner region ($r \lesssim 1$ fm) can give an equally good fit to the data.[12] Once a specific form is chosen, the data pin down the pa-

rameters of the potential very sharply.[2] Just like in the modified effective range formalism it appears that specifying the short-range potential adds unnecessary detail to the model.

For the P waves one usually has taken a simple effective range expansion where only the Coulomb interaction was included. For the $^3P_2$ wave, however, one did not parametrize the nuclear phase shift in this way, but its difference with the OPE phase shift (see Sec. II B). For the $^1D_2$ wave a more phenomenological parametrization has been used in previous analyses (see Sec. II B).

We present an analysis that has none of the above drawbacks. Theoretically well-known long-range potentials are included easily, no computational problems arise at short distances and the model dependence can be kept down to a minimum. Furthermore, all partial waves are treated with the same long-range effects (improved Coulomb, VP, OPE) included. Also the treatment of coupled channels is straightforward.

In this analysis, we use a P matrix to parametrize the short-range interaction in the lower partial waves (total angular momentum $J < 3$). The P matrix gives in a natural way a division of the interaction in a short-range and a long-range part.

Jaffe and Low[22] proposed to use the P-matrix formalism to connect multiquark states to hadron-hadron scattering, and it has been used in that sense in nucleon-nucleon scattering by Simonov[23] and Mulders.[24] The formalism is similar to the boundary condition model of Feshbach and Lomon.[25]

The P matrix is the logarithmic derivative of the radial wave function at a radius b, the P-matrix radius. It will be described in detail in the next section. For $r > b$ the interaction is described by a potential tail V. In V we wanted to include those effects that are theoretically well understood and are model independent. The electromagnetic interaction is described very accurately by the improved Coulomb potential[13,14] and the vacuum polarization potential.[26] Of the remaining long-range nuclear interaction we only took the tail of the OPE potential. It appeared not to be necessary to include shorter-range nuclear forces in the potential tail. Here the first uncertainties come into view, since the $pp\pi^0$ coupling constant is not known accurately. Fortunately enough, in this analysis it can be determined by the fit to the data. In previous analyses[2,12] the pion-coupling constant could not be determined well from the 0–30 MeV data. When an effective range model was used for the $^1S_0$ partial wave the reason was the too-crude approximation to OPE. When a potential representation was used, meaningless results for the potential parameters were obtained.[2]

Our choice for the potential tail V gives a restriction on the allowed values of b, since if b is chosen too small, $V(r)$ is no longer a good description of the pp interaction for $r > b$. Of course we could have included a two-pion-exchange potential tail, or a full nucleon-nucleon potential tail with contributions from higher-mass mesons.[27,28] This would have resulted in a more realistic potential for distances close to b. All results that change when a different (realistic) potential is taken can be termed model dependent. We have checked explicitly (Sec. VI A) that the inclusion of the heavier-boson exchanges of the Nijmegen soft-core potential[27] does not change the fit to the data. Only the P-matrix parameters change in such a way as to give, with this different potential tail, essentially the same phase shifts. Since it is thus not necessary to rely on a specific potential model for the shorter-range forces, the shortest-range potential included here is the OPE potential.

If the P matrix is parametrized as a function of the energy, one has an energy-dependent phenomenological description of the phase shifts. We used it for a multienergy (me) fit to all data published in a regular physics journal. Unfortunately enough there exist a lot of data[29–33] that have not been published in a regular physics journal, but that appeared in conference proceedings or theses only. Inclusion of these data would have changed our results (see Sec. VI). Furthermore we rejected some data on the basis of sound statistical criteria. The model, with 12 parameters, gives a statistically satisfying fit to the data. Other analyses use about the same number of parameters.

The me fit gives us the phase shifts as a function of the energy. Next to this we also did single-energy (se) fits, giving phase shifts and error matrices at certain energies. The se fits were done by clustering the data to form groups near the chosen energies. In order to do these fits, one needs some of the me results to preserve the proper energy dependence and to fix the phase shifts that cannot be fitted at the chosen energy. Single-energy phase shifts and error matrices are a representation of the data near a certain energy and are probably less model dependent than the me results. The se results can be used to judge the amount of information the data give us at different energies. They can also be used to adjust the parameters of any model for the pp interaction. The quality of such a model can then be judged from a comparison of the model's likelihood function χ^2 with our me χ^2, which is close to the expected value $\chi^2/N_{\rm df} = 1$ (Sec. V A).

We compare our results with the analyses of Sher, Signell, and Heller (SSH),[12] Noyes and Lipinski,[11] Gursky and Heller,[15] and Naisse.[2] There are other analyses that have an overlap in energy range with ours. But the series of analyses by Arndt and co-workers[34–37] and the analyses by Bystricky *et al.*[38,39] are not detailed enough for the very accurate data at low energies. The analysis by Bohannon, Burt, and Signell[40] deals with pp and np data, but only in the energy range 20–30 MeV, which contains only a small part of the 0–30 MeV pp data. Furthermore, the 20–30 MeV data are rather old and not very precise.

In Sec. II the P matrix is defined, some of its properties are given, and we describe how it is used to divide the interaction into long-range (well-known) and short-range (less well-known) interactions. We also discuss its parametrization and the choice of b. Section III is devoted to the potential tail. In Sec. IV the framework for computing the observables is given. Special attention is paid to the different kinds of phase shifts that have been used in the past and we also deal with some technical problems. In Sec. V, after a discussion of data statistics and our criteria to reject data, we enter into the details of defining

our final data set. Section VI concludes by giving our results for phase shifts and parameters. Differences between the phase shifts of our analysis and those computed with the Nijmegen soft-core potential (N78) (Ref. 27) and the parametrized Paris potential (P80) (Ref. 28) are discussed. We also give the effective range parameters that can be deduced from our results. Finally, an appendix is devoted to a test of some assumptions that were made about the data statistics.

II. THE P MATRIX, A PARAMETRIZATION IN THE LOWER PARTIAL WAVES

A. Definition and properties of the P matrix

The scattering process of two protons we describe by the relativistic[14] radial Schrödinger equation

$$\left[\frac{d^2}{dr^2}+k^2-\frac{L^2}{r^2}-M_p V(r)\right]\chi(r)=0\ , \tag{1}$$

where $\chi(r)$ is the radial wave function, M_p is the proton mass, and L^2 is shorthand notation for $l(l+1)$, with l the orbital angular momentum. The correct relativistic connection between the c.m. relative momentum k and the laboratory kinetic energy $T_{\rm lab}$ is $k^2=M_p T_{\rm lab}/2$. In the case of two coupled channels, all operators in Eq. (1) become 2×2 matrices, of which only the potential $V(r)$ is nondiagonal. The number of linearly independent solutions of Eq. (1) is twice the number of channels. But the complete physical model has only half that number of independent solutions. Therefore it consists of more than Eq. (1). For instance, in a potential model one has the boundary conditions that the physical solution is regular at the origin ($r=0$). These solutions are then written as the 2×2 matrix $\chi(r)$. Perhaps one wonders why the relativistic Schrödinger equation can provide a good relativistic description of the scattering amplitude and of bound-state energies. Then one should realize that this equation is nothing else but a differential form of the relativistic Lippmann-Schwinger (LS) integral equation. The relativistic LS equation in turn is totally equivalent with three-dimensional integral equations, such as the Blankenbecler-Sugar equation.[41–44] Important to note is that it is well known how to calculate the potential for the use in the relativistic Schrödinger equation.[45–47]

Measurements of scattering observables determine the asymptotic behavior ($r\to\infty$) of the physical solution up to an unimportant normalization. For the relation between this asymptotic behavior (definitions of phase shifts and mixing parameters) and the observable quantities, see Sec. IV.

In the P-matrix formalism[22–25] that we employ, Eq. (1) is only used for $r\geq b$, the P-matrix radius. All of the interaction inside $r=b$ is absorbed in a boundary condition at $r=b$, the P matrix

$$P(b;k^2)=b\left[\frac{d\chi}{dr}\chi^{-1}\right]_{r=b}\ . \tag{2}$$

Given the asymptotic behavior of $\chi(r)$ and the potential $V(r)$ outside $r=b$, the P matrix is uniquely determined. If b is chosen so large that the interaction outside (the long-range interaction) is well known and model independent, all models for the pp interaction that give a good fit to the data should produce the same P matrix.

If one has a model for the interaction inside $r=b$, not necessarily a potential model, the P matrix connects the physics of the inner region with the physics of the outer region. For instance, in a bag model, in which quark degrees of freedom play a role inside $r=b$, the P matrix shows poles at the energies of the eigenstates of the confined system. Jaffe and Low[22] call these eigenstates bag primitives.

We use a parametrized P matrix as a means to analyze the experimental data. We add the well-known long-range interaction by means of a potential tail and parametrize the structure of the P matrix as a function of the energy. The energy dependence of the P matrix is easier parametrized than the energy dependence of the phase shifts. The potential $V(r)$ we use for $r\geq b$ is discussed in Sec. III, and the parametrizations for the P matrix are discussed and compared with earlier partial wave parametrizations in Sec. II B. In this section we review quickly some properties of the P matrix.

P is a single-valued function of k^2. P is real for real k^2 in the case of a unitary S matrix and a Hermitian potential. In the coupled-channel case, time reversal invariance allows the choice of a symmetric potential and S matrix, leading to a symmetric P matrix.

Other important properties of the P matrix are the following.

(1) If one assumes that a local potential $V(r)$ also exists for $r<b$, one can show that the P matrix can be written as a sum of poles. In the one-channel case we may write

$$P(b;k^2)=c+k^2\sum_{n=1}^{\infty}\frac{r_n}{k^2-k_n^2}\ . \tag{3}$$

For comparison, one might look at the trivial case that $V(r)=0$ for $r<b$ and orbital angular momentum l. This leads to

$$c=l+1,\quad r_n=2,\quad k_n=z_n/b\ , \tag{4}$$

with z_n the nth zero of the spherical Bessel function $j_l(z)$.

(2) The P matrix is a decreasing function of the energy. For coupled channels this means that the derivative with respect to k^2 is a negative definite matrix. Without assumptions about the potential for $r<b$, this behavior can be seen as a consequence of classical causality,[25] but it is also possible to express it explicitly in terms of the potential in the inner region

$$\frac{dP}{dk^2}=-b[\chi^T(b)]^{-1}\int_0^b dr\,\chi^T(r)\left[1-M_p\frac{\partial V(k^2;r)}{\partial k^2}\right]\times\chi(r)[\chi(b)]^{-1}\ , \tag{5}$$

where the superscript T denotes the transpose of a matrix. From this, one can see that P is a decreasing function of the energy if the energy dependence of the potential V is not too strong. In the coupled-channel case, Eq.

(5) states that the energy derivative of P is a nonpositive matrix, provided we have a positive matrix between the square brackets.

(3) If one wants the P matrix at a different value of b, one can use the relation

$$b\frac{dP}{db}=P-P^2+b^2\left[-k^2+\frac{L^2}{b^2}+M_pV(b)\right]. \quad (6)$$

The potential tail that we use will not be entirely exact, since we do not include nuclear forces other than OPE. Furthermore, our P matrix and potential tail do not describe inelasticity. Therefore we cannot expect all of the above properties to hold exactly. We can see this by looking at the S matrix as a function of the complex energy. The S matrix has a (purely kinematical) unitarity cut, some right-hand cuts due to inelastic processes and left-hand cuts due to particle exchanges. The potential tail that we use does not contain any meson exchanges other than OPE, nor does it account for inelastic processes (couplings to channels with higher thresholds). We can only get the right S matrix if some of the cuts are still present in the P matrix. Therefore, in the P-matrix approach we might be able to spot a wrong potential tail. If one finds, e.g., for some partial wave a P matrix that increases as a function of the energy, this is an indication that the potential tail used is wrong.

The lowest-lying inelastic channels and the $T_{\rm lab}$ (in MeV) of the corresponding thresholds are $pp\pi^0(279.63)$, $d\pi^+(287.51)$, $pn\pi^+(292.30)$. We expect them to be unimportant for the P-matrix behavior in our range of energies.

Some of the left-hand cuts in the S matrix are not present in the P matrix, since we include in the potential tail the proper electromagnetic potential and the OPE potential. Thus the P matrix does not have an (improved) Coulomb singularity at $T_{\rm lab}=0$, and also the nearby cuts due to VP (starting at $T_{\rm lab}=-5.6\times10^{-4}$ MeV) and OPE (starting at -9.71 MeV) are absent in our P matrix. Since we solve the Schrödinger equation exactly for $r>b$, we expect to have included part of the iterated OPE and therefore part of the two-pion exchange (TPE). There will be left-hand cuts still present in the P matrix, of which the most nearby one starts at $T_{\rm lab}=-38.83$ MeV and is due to those TPE effects that are not included in the iterated OPE for $r>b$. In Fig. 1 the cut structure of the S and P matrix in the complex energy plane has been sketched. Due to Coulomb there is in the S matrix at $T_{\rm lab}=0$ an essential singularity and a "logarithmic" branch point, as can be seen from the $\ln(\eta')$ term in $h(\eta')$ [see Eqs. (9) and (10)]. The corresponding cut can be chosen along the negative imaginary k axis, so along the negative $T_{\rm lab}$ axis in the nonphysical plane.

B. Parametrizations in the lower partial waves

The P matrix is a description of the interaction inside $r=b$, and we will parametrize it phenomenologically. For the lower partial waves parametrization is essential, since the interaction in these partial waves is not given by improved Coulomb, VP, and OPE alone. For higher l parametrization becomes less important, since the interaction for increasing l is more and more determined by

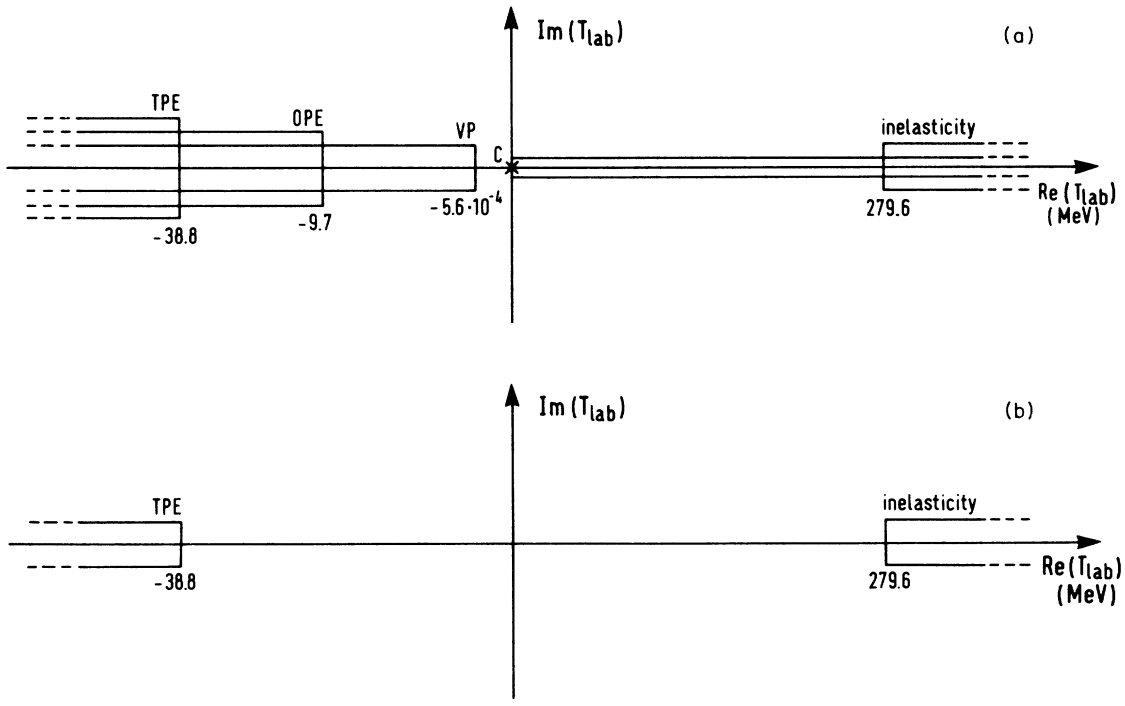

FIG. 1. (a) Cut structure of the S matrix in the complex $T_{\rm lab}$ plane. (b) Cut structure of the P matrix for the potential tail that we use in the complex $T_{\rm lab}$ plane.

the well-known long-range potential outside $r=b$. For the higher partial waves that we do not parametrize, we take the phase shifts and mixing parameters of the improved Coulomb, VP, and OPE potential, computed in Coulomb-distorted-wave Born approximation (CDWBA) (see Sec. III B). In our analysis, there was no significant improvement when F waves ($l=3$) or higher were parametrized. In this section we discuss the parametrizations of earlier analyses and of this analysis for each partial wave in which parametrization plays a role.

1. $^1S_0$

The most important wave in our low-energy range is the $^1S_0$ partial wave. It has to be treated very accurately in order to have a satisfactory description of the very accurate low-energy data. In earlier analyses two ways of parametrizing the $^1S_0$ have been used: potential representations[12,2] and (modified) effective range parametrizations.[15,16,2,17,18]

The potential parametrization approach has the advantage that well-known long-range potentials can be included exactly, but it has also several disadvantages. First of all, the form of the potential has to be known, also for intermediate and short distances. Having chosen a specific form for the potential in the inner region, the very accurate scattering data pin down the potential parameters very precisely. Different forms give for the important physical parameters (pion-coupling constant, pion mass) results that differ much more than the errors bars found. Therefore reliable estimates for the potential parameters cannot be given in this way. This is surely not the way to extract, e.g., the ppπ^0 coupling constant from the low-energy data, as is demonstrated by the analysis of Naisse.[2] Another disadvantage of potential parametrizations is that they consume much more computer time than other methods (effective range or P matrix), since the Schrödinger equation has to be solved many times for small changes in all potential parameters, in order to arrive at the parameters that are best in accordance with the data.

In the effective range method[48–51,19,52,53,17] one splits the potential V into a well-known long-range potential V_L and a remainder V_S. The phase shift δ_l can then be written as

$$\delta_l=(\delta_L)_l+(\delta_S)_l \ , \tag{7}$$

where $(\delta_L)_l$ is the phase shift of V_L. One then can define an effective range function $[F_L(k^2)]_l$ in which the left-hand singularities due to the long-range potential have been removed. For S waves one writes

$$(F_L)_0=A_0^L k\cot(\delta_S)_0+B_0^L \ , \tag{8}$$

where the functions A_0^L and B_0^L depend on the choice of V_L. In the original effective range function for the case of uncharged particles, one[50,51] used $V_L=0$. In that case $(\delta_L)_0=0$, $A_0^L=1$, $B_0^L=0$, and the corresponding effective range function is the well-known $F_0=k\cot(\delta_0)$. The most simple effective range function possible for pp scattering is obtained by taking $V_L=V_C$, the Coulomb potential.

This gives the well-known effective range function[48,49]

$$(F_C)_0=C_0^2(\eta')k\cot(\delta_0)+2k\eta' h(\eta') \ , \tag{9}$$

where δ_0 is the phase shift (with respect to Coulomb functions) of the wave function. Here η' is the standard Coulomb parameter,[54] often termed the "relativistic" η, and C_0^2 and h are the standard functions

$$\eta'=\frac{\alpha}{v_{\rm lab}}=\frac{\alpha M_p}{2k}\frac{1+2k^2/M_p^2}{(1+k^2/M_p^2)^{1/2}} \ ,$$

$$C_0^2(\eta')=\frac{2\pi\eta'}{e^{2\pi\eta'}-1} \ , \tag{10}$$

$$h(\eta')={\rm Re}[\Psi(1+i\eta')]-\ln(\eta') \ ,$$

with Ψ the digamma function. The effective range function $(F_E)_0$ when $V_L=V_C+V_{\rm VP}$ has first been given by Heller.[19] The effective range function $(F_{\rm EM})_0$ when $V_L=V_{\rm EM}$, with $V_{\rm EM}$ consisting of the improved Coulomb potential $\tilde{V}_C$ (Refs. 13 and 14) and $V_{\rm VP}$, and the effective range function $(F_{\rm OPE})_0$ when $V_L=V_{\rm EM}+V_{\rm OPE}$ have been derived by Austen[52] and van der Sanden, Emmen, and de Swart.[17] The singularity of $(F_{\rm EM})_0$ that is nearest to $k^2=0$ is a branch point, due to OPE, leading to a left-hand cut, starting at $k=\pm i m_{\pi^0}/2$ or $T_{\rm lab}=-9.71$ MeV. For low energies the standard expansion (effective range approximation) is

$$(F_{\rm EM})_0\approx-\frac{1}{a_{\rm EM}}+\frac{1}{2}r_{\rm EM}k^2 \ . \tag{11}$$

The quality of this approximation can be seen in Figs. 2 and 3, where we have plotted the shape

$$(S_{\rm EM})_0=(F_{\rm EM})_0-\left[-\frac{1}{a_{\rm EM}}+\frac{1}{2}r_{\rm EM}k^2\right] \tag{12}$$

versus $T_{\rm lab}$. For $(F_{\rm EM})_0$ and $(S_{\rm EM})_0$, see also Secs. VI A and VI B where $(S_{\rm EM})_0$ is used to display results for the $^1S_0$ partial wave (Sec. VI A) and to present the effective range parameters that can be deduced from the very-low-energy behavior of our $^1S_0$ phase shift (Sec. VI B). From Figs. 2 and 3 it is readily seen that the effective range approximation Eq. (11), equivalent with the approximation $(S_{\rm EM})_0=0$, is clearly not in accordance with the experiments, not even for the lowest energies. However, when one is not interested in a high-accuracy description, then the approximation Eq. (11) gives in the energy region $T_{\rm lab}\lesssim 50$ MeV the effective range function $(F_{\rm EM})_0$ up to $\pm 2.5\%$. In Fig. 2 two effects are noticeable. In the very-low-energy region one can see that $(S_{\rm EM})_0$ is negative and bending down, which is almost completely due to the most nearby singularity in the complex energy plane, OPE. For higher energies $(S_{\rm EM})_0$ has to bend upward, because it has to rise to $+\infty$ at $T_{\rm lab}\approx 250$ MeV, where the phase shift is crossing zero, turning negative. That the phase shift turns negative is in potential models a consequence of the repulsive core. The deviations of the effective range function from a straight line were first treated in the Cini-Fubini-Stanghellini (CFS) approxima-

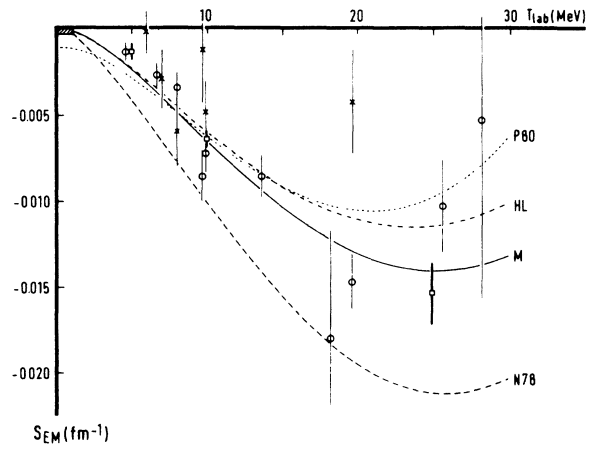

FIG. 2. The shape S_{EM} vs T_{lab}. S_{EM} is defined in Eqs. (12) and (76), using a_{EM} and r_{EM} of our me fit. ⊕:,single-energy analyses. *M*: multienergy analysis. P80: Paris potential (Ref. 28). N78: Nijmegen potential (Ref. 27). ϕ: single-group analyses. The points marked with ✳ are the single-group results of the (unpublished) Minnesota77 (Refs. 29 and 30) data. The dashed line (HL) displays the me fit if the Minnesota77 and the Los Alamos76 (Refs. 31 and 32) data are included.

tion.[20,21] In this approximation the left-hand cut of the Born approximated $l=0$ partial wave amplitude was approximated for low energies by one pole. For $(F_{EM})_0$ this results in the CFS1 approximation

$$(F_{EM})_0=-\frac{1}{a_{EM}}+\frac{1}{2}r_{EM}k^2-\frac{Pk^4}{1+Qk^2}\ , \tag{13}$$

where P and Q are complicated functions of a_{EM}, r_{EM}, the pion mass m_{π^0}, the pion-coupling constant $g^2_{pp\pi^0}$, and if Coulomb effects are taken into account, of the strength of the Coulomb potential. Not counting the pion-coupling constant as a parameter, Eq. (13) contains two

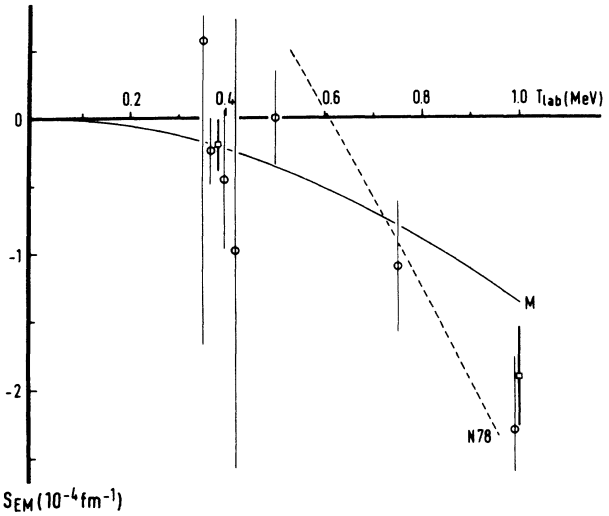

FIG. 3. Enlarged display of the shaded region in Fig. 2. The Paris potential cannot be seen, since its phase shift is too large at low energies.

parameters: a_{EM} and r_{EM}. Since the CFS1 parametrization does not allow $(S_{EM})_0$ to bend back, this description of the $^1S_0$ phase shift becomes rapidly very bad (the shape only grows more negative) for energies $T_{lab}\geq 5\sim 10$ MeV. For energies below about 2 MeV this approximation does not produce enough shape. With the pion-coupling constant as a parameter, this can be mended for very low energies by enlarging $g^2_{pp\pi^0}$ and for higher energies by reducing it. This effect can be seen clearly in Table V of the analysis by Naisse.[2] To repair the features of the shape function for higher energies a CFS2 approximation has been proposed,[52] where

$$(F_{EM})_0=-\frac{1}{a_{EM}}+\frac{1}{2}r_{EM}k^2-\frac{P'k^4}{1+Q'k^2}\frac{(1-ck^2)}{(1-dk^2)}\ . \tag{14}$$

In this approximation the parameter c allows for $(S_{EM})_0=0$ at $T_{lab}\approx 40$ MeV and the constant d is fixed to have a zero phase shift at $T_{lab}\approx 250$ MeV. Therefore d does not necessarily have to be regarded as a parameter for our range of energies. P' and Q' can again be calculated in terms of a_{EM}, r_{EM}, c, d, m_{π^0}, and $g^2_{pp\pi^0}$. Not counting the pion-coupling constant as a parameter, Eq. (14) contains thus three parameters. The CFS2 approximation is able to describe the features of $(S_{EM})_0$ discussed above and shown in Figs. 2 and 3. But still this approximation is not good enough, because it requires too-large values for the $pp\pi^0$ coupling constant. By analyzing $^1S_0$ phase shifts below 30 MeV of a nucleon-nucleon potential it has been shown[52] that the CFS2 parametrization gives a pion-coupling constant that is about 20% too large. Since the pion-coupling constant can be determined from the low-energy data with about 10% accuracy, the CFS2 approximation is not good enough.

In order to treat OPE better, a pion-modified effective range function $(F_{OPE})_0$ has been derived,[52,17] where the long-range potential is taken to be $V_L=V_{EM}+V_{OPE}$. This function $(F_{OPE})_0$ does not contain the left-hand cut due to OPE. For $(F_{OPE})_0$ the approximation is used[52,17]

$$(F_{OPE})_0=-\frac{1}{a_{OPE}}+\frac{1}{2}r_{OPE}k^2-\frac{P_{OPE}k^4}{1+Q_{OPE}k^2}\ . \tag{15}$$

Values for P_{OPE} and Q_{OPE} are fitted with the restriction that the $^1S_0$ phase shift is zero at $T_{lab}\approx 250$ MeV, so Eq. (15) contains three parameters for the low-energy region, if one does not count the pion-coupling constant. It gives a good description of the $^1S_0$ phase shift and reproduces the input pion-coupling constant of the potential within about 2%. The main problem with the pion-modified effective range treatment for the $^1S_0$ is that great care has to be taken to get sufficient accuracy. The problem is due to the singular behavior at $r=0$ of the long-range potential $V_L=\tilde{V}_C+V_{VP}+V_{OPE}$. From all solutions with asymptotically equal norm a specific irregular solution has to be defined by its behavior around $r\approx 0$. Since irregular solutions blow up at $r\approx 0$, small numerical errors made in this behavior around $r\approx 0$ mean an unwanted admixture of the (much smaller) regular wave function.

Since the regular and the irregular solution have the same norm asymptotically, the small errors made around $r \approx 0$ grow more important for larger r.

The main problems in analyses that use potential parametrizations or effective range parametrizations are thus due to the inner region of the interaction. The P-matrix parametrization that we employ here combines the merits of the former methods and lacks their problems. At the end of this section an overview is given of these advantages for all partial waves.

The $^1S_0$ appeared to be well described by the one-pole P-matrix parametrization

$$P(k^2)=c_0+\frac{r_0 k^2}{k^2-k_0^2}\ , \tag{16}$$

with the three parameters c_0, r_0, and k_0. Of course, also the pion-coupling constant that affects all partial waves and the P-matrix radius b that affects the lower partial waves contribute in the parametrization of the $^1S_0$.

The $^1S_0$ P matrix does not need more parameters in this energy range. One can see that the one-pole parametrization is a natural low-energy version of Eq. (3), since for low energies higher poles add up to a background P matrix that can be absorbed in the constant c_0. To analyze a larger energy region one would need a more detailed parametrization than Eq. (16). This can be seen, e.g., by fitting the three $^1S_0$ P-matrix parameters under the constraint that $\delta(^1S_0)=0$ at 240 MeV.[36] This raises the minimal χ^2 ($\chi^2_{\min}$) on the low-energy data by about 9. Our $^1S_0$ phase parametrization turns out to be able to give the same results as the pion-modified effective range parametrization of van der Sanden, Emmen, and de Swart[17] up to 30 MeV, i.e., the difference between the two methods is much less than the spread in the data. This is a very nice result, since the phenomenological parametrization of the short-range interaction is accomplished in a different way in the two methods.

2. $^3P_0$, $^3P_1$, and $J=2$ coupled channel $^3P_2$-ϵ_2-$^3F_2$

For the P waves, the analyses of SSH[12] and Naisse[2] use the uncoupled, Coulomb-modified two-term effective range approximations

$$\begin{aligned}(F_C)_{1J}&=k^2(1+\eta'^2)[C_0^2(\eta')k\cot(\delta'_{1J})+2k\eta' h(\eta')]\\&=-\frac{1}{a_{1J}}+\frac{1}{2}r_{1J}k^2\quad(J=0,1,2)\ .\end{aligned}\tag{17}$$

For $J=0,1$ the phase shift δ'_{1J} is taken to be δ^C_{1J}, the phase shift one would have if the only electromagnetic interaction present were the $1/r$-shaped Coulomb. For a definition of δ^C_{lJ} see Sec. IV B. One cannot use the same procedure for the $^3P_2$, since the anomalous threshold behavior of the $^3P_2$ phase shift gives this effective range function a structure different from a straight line as a function of $T_{\rm lab}$. Therefore both analyses[12,2] use

$$\delta'_{12}=\delta^C_{12}-C_0^2(\eta')(1+\eta'^2)\delta^{\rm OPE}_{12}\tag{18}$$

In this rather *ad hoc* subtraction, the OPE phase shift for uncharged particles $\delta^{\rm OPE}_{12}$ is multiplied with the Coulomb penetration factor. This approximation to the pp OPE $^3P_2$ phase shift is not good enough. In the analysis of van der Sanden, Emmen, and de Swart[17] a better pp OPE $^3P_2$ phase shift is subtracted, being the CDWBA to the OPE $^3P_2$ phase shift. In Fig. 4 it can be seen that the linear approximation to $(F_C)_{12}$ [Eq. (17)] with the CDWBA to the OPE $^3P_2$ phase shift is better than with the BA. With potential phase shifts as input, it has been shown[55] that using the BA leads to a pion-coupling constant that is about 10% higher than the input value.

For the $^3P_0$ and $^3P_1$ Eq. (17) is a satisfactory parametrization, the only drawback is that the $^3P_0$ and $^3P_1$ do not determine the pion-coupling constant at all. The connection of the $^3P_2$ with the pion-coupling constant in Eq. (18) is very indirect. One cannot avoid the problem in the $^3P_2$ by using a Coulomb-modified effective range approximation for the standard low-energy combinations of P-wave phases Δ_C, Δ_T, and $\Delta_{\rm LS}$, since $\Delta_C=0$ for $T_{\rm lab}\approx 8$ MeV, and therefore the effective range function is infinite. These P-wave phase shift combinations are defined by

$$\begin{aligned}\Delta_C&=\tfrac{1}{9}(\delta_{10}+3\delta_{11}+5\delta_{12})\ ,\\ \Delta_{\rm LS}&=\tfrac{1}{12}(-2\delta_{10}-3\delta_{11}+5\delta_{12})\ ,\\ \Delta_T&=\tfrac{5}{72}(-2\delta_{10}+3\delta_{11}-\delta_{12})\ ,\end{aligned}\tag{19}$$

where the standard notation δ_{lJ} is used for the ^3P_J phase shifts. To solve the problem with the $^3P_2$, one could try a pion-modified effective range function, but since the OPE potential couples the $^3P_2$ to the $^3F_2$ via the tensor force, one would need a coupled-channels effective range matrix.[56,57] Of course this gives even more numerical accuracy problems than in the $^1S_0$ case, but more important is that one has to introduce at least one parameter (scattering length) for the $^3F_2$ since the no-interaction (parameter-free) effective range function is singular. Since the difference of the $^3F_2$ phase shift and the ϵ_2 mixing parameter with the OPE values is hardly to be seen below 30 MeV, this parameter is not determined by the data.

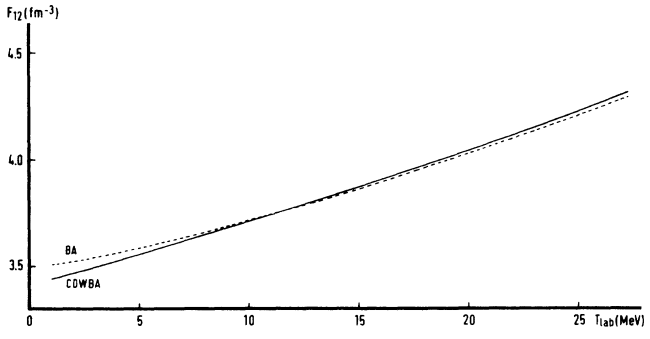

FIG. 4. $^3P_2$ effective range function F_{12} [Eqs. (17) and (18)] vs $T_{\rm lab}$ for the Nijmegen78 potential (Ref. 27). BA: The Born approximation to its $\delta^{\rm OPE}_{12}$ and Coulomb penetration factor. CDWBA: The Coulomb-distorted-wave BA to its $\delta^{\rm OPE}_{12}$.

All of the above problems are solved by the P-matrix method. A two-parameter description appeared to be necessary. The linear approximation that we use for the uncoupled P waves

$$P(k^2)=c_{1J}+d_{1J}k^2 , \tag{20}$$

with $J=0,1$ for the $^3P_0$, $^3P_1$, respectively, can be seen as a natural low-energy version of Eq. (16) if the pole is far away.

Also for the $J=2$ coupled channels $^3P_2$-ϵ_2-$^3F_2$ two parameters are sufficient, so we use

$$P(k^2)=\begin{bmatrix} c_{12}+d_{12}k^2 & 0 \\ 0 & c_{32} \end{bmatrix} , \tag{21}$$

with $c_{32}=4$. One can see that all matrix elements, except for the upper-diagonal one have been set to the $T_{\rm lab}=0$ limit of the P matrix without interaction inside $r=b$ [Eqs. (3) and (4)]. This coupled approximation with no parameters for the ϵ_2 or $^3F_2$ corresponds almost exactly to giving the ϵ_2 and $^3F_2$ their OPE values.

3. $^1D_2$

The $^1D_2$ needs only one parameter up to 30 MeV. In the analyses of SSH,[12] Naisse,[2] and van der Sanden, Emmen, and de Swart[17] the approximation for the $^1D_2$ phase shift used looks like

$$\delta_2^{\rm EM}=\delta_2^{\rm OPE}(1+\gamma T_{\rm lab}) . \tag{22}$$

For the definition of the electromagnetic phase shift $\delta_l^{\rm EM}$ (phase shift with respect to electromagnetic wave functions) see Sec. IV B. The analyses of SSH[12] and Naisse[2] take $\delta_2^{\rm OPE}$ to be the OPE phase shift for uncharged particles. Analyzing potential phase shifts, it has been shown[55] that this neglection of Coulomb effects leads to a prediction of the pion-coupling constant that is about 10% too low, as can be seen in Fig. 5. Correcting the above $\delta_2^{\rm OPE}$ with only the Coulomb penetration factor leads to a prediction that is about 10% too high (Fig. 5). Therefore, van der Sanden, Emmen, and de Swart[17] calculate $\delta_2^{\rm OPE}$ using the CDWBA. We use the natural one-parameter approximation limit of Eq. (20)

$$P(k^2)=c_2 . \tag{23}$$

Counting the parameters used we arrive at 10 P-matrix parameters plus the P-matrix radius b for the lower partial waves, and the pion-coupling constant that affects all partial waves. Of these, b does not necessarily have to be regarded as being a parameter, since it is not well determined by the low-energy data. As a parameter, b can be compared in some sense with the parameter that effective range analyses use to ensure the good high-energy behavior of the $^1S_0$ phase shift. Of these two parameters, the P-matrix radius b has a more direct physical interpretation. Because the long-range interaction that we use is only adequate for not too small r, b cannot be chosen too small. From Eqs. (3) and (4) one can see that large values of b shift the pole positions to lower energies. Our parametrizations do not allow for too much structure, so b cannot be chosen too large. In order to have a realistic model, we have to add the restriction that b must be somewhat larger than the range of interactions that we did not include in the potential tail. So we want b to be larger than about 1 fm, larger than the range of the two-pion exchange. Therefore we expect to find some allowed range of values for b.

From the P-matrix property Eq. (5) that P is a decreasing function of the energy, it can be expected that $r_0>0$ and $d_{1J}<0$. By comparing the parameters c_0, c_{1J}, and c_2 with the free values $c_{lJ}=l+1$, one can judge the amount of effective short-range interaction. If the short-range interaction is not so attractive that the P matrix has poles below threshold, then one can see that an attractive short-range interaction makes the P matrix more negative than its free value, while a short-range repulsion makes it more positive.

As a conclusion to this section, we give a quick resumé of the advantages of the P-matrix method over the previously used (modified) effective range and potential parametrization methods. Well-known long-range interactions are included easily. The radial Schrödinger equation has to be solved only a few times for each energy (see Sec. III). No computational problems arise at short distances. The phenomenology, necessary to describe accurately the short- and intermediate-range interaction, is not mixed up with the well-known long-range interaction. The treatment of the $J=2$ coupled channels is straightforward, since a coupled-channels parametrization is available that uses no parameters for the ϵ_2 and $^3F_2$. All lower partial waves are treated with the same theoretically well-known long-range effects (improved Coulomb, VP, OPE) included, since we use the same potential outside $r=b$. In Sec. III B, where the treatment of the higher partial waves is explained, it is shown that all these long-range effects are also taken into account in the higher partial waves. Therefore, e.g., the pion-coupling constant is determined from all partial waves in a natural way.

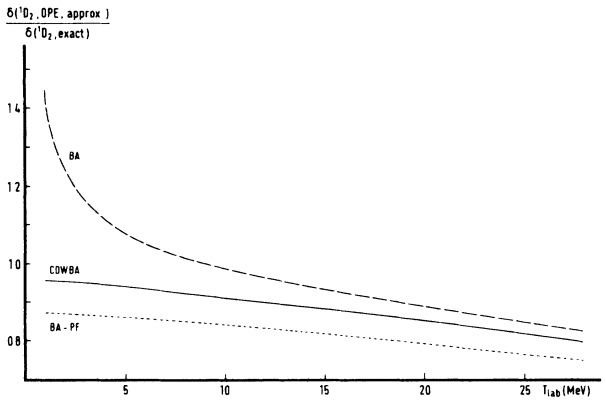

FIG. 5. Different approximations to the $^1D_2$ phase shift of the OPE part of the Nijmegen78 potential [Eq. (31) of Ref. 27], divided by the $^1D_2$ phase shift of the Nijmegen78 potential. BA: Born approximation. BA-PF: BA with Coulomb penetration factor. CDWBA: Coulomb-distorted-wave BA.

III. THE POTENTIAL TAIL

A. Defining the potential

As we employ the P-matrix formalism we only need a potential tail in the region $r > b$. Thus only the longest-range interactions have to be included in the potential. The higher partial waves are determined almost completely by the long-range interaction and can therefore be produced by the potential tail alone. For all partial waves we use the same potential tail

$$V = V_{\rm OPE} + V_{\rm EM} = V_{\rm OPE} + \tilde{V}_C + V_{\rm VP} \ , \tag{24}$$

where $V_{\rm OPE}$ is the one-pion-exchange potential and $V_{\rm EM}$ is the electromagnetic potential consisting of the improved Coulomb potential $\tilde{V}_C$ and the vacuum polarization potential $V_{\rm VP}$.

The improved Coulomb potential[13,14] takes into account the lowest-order relativistic corrections to the static Coulomb potential and includes contributions of all two-photon-exchange diagrams. As will be discussed later, we can neglect in our energy range the spin-orbit and tensor parts of this potential. We take the "gauge" parameter $\lambda = 0$, resulting in[14]

$$\begin{aligned} \tilde{V}_C &= V_{C1} + V_{C2} \ , \\ V_{C1} &= \alpha'/r \ , \\ V_{C2} &= -\frac{1}{2M_p^2}\left[(\Delta + k^2)\frac{\alpha}{r} + \frac{\alpha}{r}(\Delta + k^2)\right] \ , \end{aligned} \tag{25}$$

where Δ is the Laplacian and α' is given by

$$\alpha' = \frac{2k\eta'}{M_p} \ , \tag{26}$$

with η' given by Eq. (10). The most important difference with the standard static Coulomb potential is the use of α' instead of α.

The vacuum polarization potential $V_{\rm VP}$, as derived by Uehling[58] and reviewed by Durand,[26] can be written as

$$V_{\rm VP} = \frac{2\alpha}{3\pi}\frac{\alpha'}{r}\int_1^\infty dx\, e^{-2m_e rx}\left[1 + \frac{1}{2x^2}\right]\frac{(x^2-1)^{1/2}}{x^2} \ . \tag{27}$$

Here m_e is the electron mass and α and α' are as given above. The unprimed α describes the coupling of a photon to the virtual e^+e^- pair, the α' the coupling to the protons.

For one-pion exchange several potentials could be used, which differ only at short distances, due to the choice of different form factors. Since we only need the tail of the potential, we took the simple form

$$V_{\rm OPE} = \frac{1}{3}\frac{g^2_{{\rm pp}\pi^0}}{4\pi}\frac{M_p}{(M_p^2+k^2)^{1/2}}\frac{m^3}{4M_p^2}\frac{e^{-mr}}{mr} \times\left[(\sigma_1\cdot\sigma_2) + S_{12}\left[1 + \frac{3}{(mr)} + \frac{3}{(mr)^2}\right]\right] \ , \tag{28}$$

where m is the π^0 mass and $g^2_{{\rm pp}\pi^0}/4\pi$ is the ${\rm pp}\pi^0$ coupling constant. This coupling constant is not known accurately. From pion-nucleon scattering one knows the ${\rm NN}\pi^\pm$ coupling, but the ${\rm pp}\pi^0$ coupling could well be different. Besides, we are here in a totally different kinematic region. The best place to determine the ${\rm pp}\pi^0$ coupling constant is probably in pp scattering. For that reason, we have fitted in this analysis the coupling constant to the data. Since $g^2_{{\rm pp}\pi^0}$ is extracted only from the tail of the interaction where no theoretical uncertainties exist, we believe that this is a rather model-independent determination (see also Sec. VI).

We now quickly review the effects we included in our potential tail, in order of diminishing strength. The potential V_{C1} of Eq. (25) is the dominant interaction for small scattering angles, especially at low energies. At $T_{\rm lab} = 10$ MeV, the Coulomb potential still dominates for c.m. angles below 20° which makes it imperative to include it. The importance of the one-pion-exchange tail can be seen from the fact that from the data its coupling constant is determined with about 10% accuracy. Therefore, if the effect would be entirely neglected, corresponding to a zero coupling constant, no good fit to the data could be expected. We have explicitly checked the importance of the vacuum polarization by completely removing it from our model. This means that it was left out of the potential tail and, as explained above, was no longer present in any partial wave. After that, all model parameters were refitted. The resulting minimal χ^2 then remains higher by ~ 100, compared with the complete model. The vacuum polarization is thus seen in the data with a significance of 10 standard deviations (s.d.).

In the same way we tested the use of α' instead of α. The use of α gives in our final fit to the data an increase in χ^2 of about 20, so this effect has a significance of 4.5 s.d.

The term V_{C2} of Eq. (25) does not give a significantly better fit. The magnitude of this effect is about 10 times smaller than the vacuum polarization, as can be seen, for instance, from the phase shifts (Sec. IV). Still we do not want to neglect this effect, because its presence will slightly influence the energy dependence that our model can give to the phase shifts. Especially the threshold behavior of the $^1S_0$ phase shift near $T_{\rm lab} = 0$ will only be correct if the long-range interactions are treated correctly.

Finally we mention the magnetic moment interactions. As was stated earlier, we neglect these terms of the potential. The reason is that these interactions are again ~ 10 times smaller than V_{C2}. The magnetic moment interaction in the $^1S_0$ partial wave is a δ function in the origin and is therefore included in the short-range interaction, which is described by the P matrix. In the P waves its phase shifts are less than 10^{-4} deg. A detailed treatment of this effect can be found in Ref. 59, where its importance is also found to be negligible.

B. Calculations

In order to see how the potential tail is used in our model, we first turn to those partial waves that have a

parametrized P matrix. For these waves, the P-matrix value for a certain energy is given by the parametrization. Knowing the P matrix is enough to give the radial wave function and its derivative χ and χ' at $r=b$ up to a common normalization factor. The Schrödinger equation enables us then to compute $\chi(r)$ for all $r>b$. This wave function will, for very large r, have the asymptotic behavior

$$\chi(r) \underset{r\to\infty}{\sim} F_l(\eta',kr)C_1+G_l(\eta',kr)C_2 \ , \tag{29}$$

where F_l and G_l are the regular and irregular Coulomb functions as defined in Ref. 60 and η' is as defined in Eq. (10). In the nucleon-nucleon interaction the spin-triplet states with $J=l\pm1$ are coupled. In that case Eq. (29) becomes a matrix equation. The 2×2 matrix χ consists then of columns which are independent two-component solutions, and F_l and G_l become diagonal matrices. The coefficients (matrices) C_1 and C_2 of Eq. (29) contain all necessary information about the partial wave. In terms of C_1 and C_2, the K matrix and S matrix are defined as

$$K_J=C_2C_1^{-1}, \quad S_J=\frac{1+iK_J}{1-iK_J} \ . \tag{30}$$

In Sec. IV A the decomposition of the S matrix into phase shifts will be discussed.

In practice, the calculations have to be repeated many times while the P-matrix parameters are fitted. Because it would be rather time consuming, it is not desirable to solve the Schrödinger equation each time to compute the asymptotic behavior of χ. For each energy, we need only once to compute two independent solutions $\chi_1(r)$ and $\chi_2(r)$ of the wave equation, satisfying the boundary conditions at $r=b$

$$\begin{aligned} &\chi_1(b)=1, \quad \frac{d}{dr}\chi_1(b)=0 \ , \\ &\chi_2(b)=0, \quad \frac{d}{dr}\chi_2(b)=1 \ . \end{aligned} \tag{31}$$

Their asymptotic behavior for $r\to\infty$ is given by

$$\begin{aligned} &\chi_1(r)=F_l(\eta',kr)A+G_l(\eta',kr)B \ , \\ &\chi_2(r)=F_l(\eta',kr)C+G_l(\eta',kr)D \ . \end{aligned} \tag{32}$$

For any P matrix P, we then can compute C_1 and C_2 of Eq. (29)

$$C_1=A+CP/b, \quad C_2=B+DP/b \ . \tag{33}$$

The coefficients A, B, C, and D have to be computed for each parametrized partial wave and for all energies appearing in the data set. A complication arises if the potential tail contains parameters, as in our case the pion-coupling constant $g^2_{pp\pi^0}$. We solved this by interpolating each coefficient, using computed values for three different values of $g^2_{pp\pi^0}$.

The improved Coulomb potential [Eq. (25)] cannot be used directly in a radial wave equation. It contains a nonlocal potential of the form

$$V(r)=V_0(r)-1/M_p[\Delta\phi(r)+\phi(r)\Delta] \ . \tag{34}$$

A widely used method to deal with this problem is to define

$$\bar{\chi}(r)=\sqrt{1+2\phi(r)}\chi(r) \ . \tag{35}$$

The function $\bar{\chi}$ then is a solution of the normal radial Schrödinger equation with the local potential

$$W=\frac{V_0}{1+2\phi}+\frac{1}{M_p}\left[\frac{2\phi k^2}{1+2\phi}-\frac{\phi'^2}{(1+2\phi)^2}\right] \ . \tag{36}$$

For any P matrix, one can compute the boundary condition for $\bar{\chi}$ with Eq. (35). Writing $\bar{\chi}$ as a linear combination of χ_1 and χ_2, Eqs. (30), (32), and (33) give then the S matrix [if $\phi(r)\to0$ sufficiently fast for $r\to\infty$].

We mentioned before that for the partial waves with higher angular momentum, we would like to use fixed phase shifts that are produced by our chosen potential tail. The higher partial wave phase shifts are very insensitive to the short-range potential. Whether one adds to the potential tail $V(r)$ of Eqs. (24)–(28) a zero potential for $r<1.4$ fm or one adds a form factor continuation of $V(r)$ for $r<1.4$ fm, gives at 30 MeV only a difference of 10^{-3} deg in the $\delta(^3F_4)$, 2×10^{-4} deg in the $\delta(^3F_3)$, and even less in the other (higher) partial waves. Thus for the partial waves with $l\geq3$ any reasonable choice for the short-range part of the potential would give the same result. One does not have to solve the Schrödinger equation in the higher partial waves, as the BA or the CDWBA will get accurate enough as l increases. This is shown in Table I, where we give the $^3F_3$, $^3F_4$, and $^1G_4$ phase shifts and the ϵ_4 mixing parameter computed for the α'/r Coulomb potential plus the $V_{\rm OPE}$ with a form factor continuation inside $r=1.4$ fm ($C+$OPE), and the BA and CDWBA to these phase shifts and mixing parameter.

In our fits we use for $J\geq3$ the CDWBA, which is seen to be a more accurate approximation to the K-matrix elements than the BA. The computation of CDWBA phase shifts leads to integrals for the partial wave K-matrix elements

$$K_{l',l}=-\frac{M_p}{k}\int_0^\infty dr\, F_{l'}(\eta',kr) \times(V_{C2}+V_{\rm VP}+V_{\rm OPE})F_l(\eta',kr) \ . \tag{37}$$

$V_{\rm OPE}$ consists of terms of the type e^{-mr}/r^n. Integrals of these functions between Coulomb functions can be

TABLE I. $^3F_3$, $^3F_4$, and $^1G_4$ phase shifts and ϵ_4 mixing parameter (in degrees) at $T_{\rm lab}=30$ MeV of the potential $V_{C1}+V_{\rm OPE}$ [Eqs. (25) and (28)] with a form factor continuation for $r<1.4$ fm and $g^2_{pp\pi^0}/4\pi=14.4$. BA and CDWBA: Born approximation and Coulomb-distorted-wave Born approximation to the $C+$ OPE values.

	$C+$ OPE	BA	CDWBA
$\delta(^3F_3)$	−0.3424	−0.3583	−0.3463
$\delta(^3F_4)$	0.0266	0.0254	0.0243
ϵ_4	−0.0775	−0.0797	−0.0774
$\delta(^1G_4)$	0.0619	0.0637	0.0618

computed accurately in a fast and elegant way using recursion relations.[55] The other two potentials, V_{C2} and V_{VP}, do not couple partial waves with different angular momentum, thus for their contribution to the K matrix in Eq. (37) one needs only to consider $l'=l$. For the contribution of V_{VP} one can use the results of Durand.[26] In our calculations we used an expansion in $\log(T_{lab})$, like Eq. (8.3) of Durand, but with more terms to extend the energy range to lower energies. To compute the contribution of V_{C2} [Eq. (25)] we consider first the operator $\Delta+k^2$. From the three-dimensional wave equation with potential V_{C1}

$$(\Delta+k^2)\psi(\mathbf{r})=M_p V_{C1}(r)\psi(\mathbf{r}) \tag{38}$$

follows that in CDWBA the operator $\Delta+k^2$ is equivalent with $M_p V_{C1}=M_p\alpha'/r$. Therefore the contribution of the potential V_{C2} in Eq. (37) can be written as (suppressing some arguments)

$$\int_0^\infty dr\, F_l V_{C2} F_l = -\frac{\alpha\alpha'}{M_p}\int_0^\infty dr \frac{F_l^2}{r^2} . \tag{39}$$

In CDWBA the potential V_{C2} is therefore equivalent with $V'_{C2}=-\alpha\alpha'/M_p r^2$. The Schrödinger equation with the potential $V_{C1}+V'_{C2}$ can be solved exactly, because V'_{C2} can be absorbed in the centrifugal barrier. The solution is a regular Coulomb function $F_{l'}$ with $l'\approx l-\alpha\alpha'/(2l+1)$ up to leading order in α. The phase shift ρ_l of V'_{C2} can be obtained from the asymptotic behavior of the regular Coulomb function

$$F_l(\eta',kr) \underset{r\to\infty}{\sim} \sin\left[kr-\frac{\pi l}{2}+\sigma_l-\eta'\ln(2kr)\right] , \tag{40}$$

where

$$\sigma_l=\arg[\Gamma(l+1+i\eta')] . \tag{41}$$

Then one finds that in very good approximation

$$\rho_l \approx \frac{\alpha\alpha'}{2l+1}\left[\frac{\pi}{2}-\frac{d\sigma_l}{dl}\right]$$

$$=\frac{\alpha k}{M_p}\frac{1}{2l+1}\left[1-C_0^2(\eta')+2\eta'^2\sum_{j=1}^{l}\frac{1}{\eta'^2+j^2}\right] , \tag{42}$$

with $C_0^2(\eta')$ as given by Eq. (10).

IV. PHASE SHIFTS AND AMPLITUDES

A. Basic definitions

In order to define phase shifts for an interaction which contains the Coulomb force, one has to match the wave function asymptotically to Coulomb functions [Eq. (29)]. One then defines the K and S matrix by Eq. (30). For an uncoupled channel the phase shift δ is defined by $\tan\delta=K$ or $S=e^{2i\delta}$. In the case of two coupled channels we use the "bar" phase shifts,[61] defined by

$$S_J=\begin{pmatrix} e^{i\delta_1} & \\ & e^{i\delta_2}\end{pmatrix}\begin{pmatrix}\cos2\epsilon_J & i\sin2\epsilon_J \\ i\sin2\epsilon_J & \cos2\epsilon_J\end{pmatrix}\begin{pmatrix} e^{i\delta_1} & \\ & e^{i\delta_2}\end{pmatrix} . \tag{43}$$

This is possible because the S matrix is unitary and symmetric. The phase shifts δ_1 and δ_2 are usually denoted as δ_{lJ}, so $\delta_{J-1,J}$ and $\delta_{J+1,J}$, respectively. For the uncoupled channels one uses δ_l to denote the spin-singlet phase shift and δ_{ll} for the uncoupled triplet, which has $l=J$.

Because we deal with identical particles the amplitude, or M matrix, in the spin space of both particles must be symmetrized. This results in

$$\langle s,m' \mid M(\theta,\phi) \mid s,m\rangle = \langle sm' \mid M_C(\theta) \mid s,m\rangle$$

$$+2\sum_{\substack{l',J,l \\ s+l \text{ even}}} Y^{l'}_{m-m'}(\theta,\phi) C^{l' \; s \; J}_{m-m' \; m' \; m} i^{l-l'} e^{i\sigma_{l'}} \frac{\langle l',s \mid S_J-1 \mid l,s\rangle}{2ik} e^{i\sigma_l} C^{l \; s \; J}_{0 \; m \; m}\sqrt{4\pi(2l+1)} , \tag{44}$$

where $C^{l\ s\ J}_{m_l\ m_s\ M}$ is a Clebsch-Gordan coefficient and $Y^l_m(\theta,\phi)$ is a spherical harmonic. The σ_l are the Coulomb phase shifts, defined up to an unimportant, l-independent constant (see Refs. 62 and 63) by Eq. (41).

The symmetrized Coulomb M matrix for proton-proton is

$$\langle s,m' \mid M_C(\theta) \mid s,m\rangle = \delta_{m'm}[f_C(\theta)+(-1)^s f_C(\pi-\theta)] , \tag{45}$$

where

$$f_C(\theta)=-\frac{\eta'}{2k}\frac{e^{2i\sigma_0}}{[\sin^2(\theta/2)]^{1+i\eta'}} . \tag{46}$$

All scattering observables can be expressed in terms of the M matrix.[64,65]

B. Different types of phase shifts

The kind of phase shifts defined above are unfortunately not the only ones in use. To compare our results with other publications, we have to introduce some other kinds as well. A phase shift, as the word says, is a shift of

one wave function with respect to another. For the kind of phase shifts in Sec. IV A these functions are the physical wave function χ and the Coulomb wave function F_l, respectively. Since each choice for the interaction leads to a particular regular wave function, we can define phase shifts of different interactions (or potentials) with respect to each other. For the moment we disregard coupled channels and suppress the indices l and J.

We denote by δ_W^V the phase shift of the solution with potential W with respect to the solution with V as the interaction. We apply this to the case where we have a potential consisting of a Coulomb potential $V_C=\alpha'/r$, some additional electromagnetic corrections $V_{\rm EMC}$, and the nuclear part V_N. The phase shifts as defined in Sec. IV A, which were denoted as δ, can now be fully denoted as $\delta_{C+{\rm EMC}+N}^C$. We keep the short notation as an alternative. We now use

$$\delta_{C+{\rm EMC}+N}^C=\delta_{C+{\rm EMC}+N}^{C+{\rm EMC}}+\delta_{C+{\rm EMC}}^C \ . \tag{47}$$

The $\delta_{C+{\rm EMC}+N}^{C+{\rm EMC}}$ are also denoted as $\delta^{\rm EM}$. They are called phase shifts with respect to electromagnetic wave functions, or nuclear-electromagnetic phase shifts. The first name expresses that they can also be defined using Eqs. (29), (30), and (43) with F_l and G_l replaced by a regular and irregular solution for the potential $V_C+V_{\rm EMC}$.

The phase shifts $\delta^{\rm EM}$ are useful because, as we will show later, they can speed up the summation involved in Eq. (44). One more reason to define them is their appearance in effective range functions to extend the region of convergence of the effective range series. A difficulty is that the definition of the $\delta^{\rm EM}$ depends on the choice of the potential $V_{\rm EMC}$. If the correction $V_{\rm EMC}$ only consists of the vacuum polarization potential $V_{\rm VP}$, it gives the so-called nuclear-electric phase shifts, denoted by a superscript E. They satisfy

$$\delta_l=\delta_l^E+\tau_l \ , \tag{48}$$

where τ_l is the vacuum polarization phase shift. Often more effects are included in $V_{\rm EMC}$. For instance SSH[12] included magnetic moment interactions and finite size effects. However, they still denoted their nuclear-electromagnetic phase shifts with a superscript E. They also used an effective range formula that was meant to be used with phase shifts δ^E. In our analysis we neglect magnetic moment interactions, as explained in Sec. III A. We also do not include finite-size effects, since the entire short-range interaction is parametrized. Our $V_{\rm EMC}$ consists of $V_{\rm VP}$ and V_{C2} [Eqs. (24), (25), and (27)], which leads to

$$\delta_l=\delta_l^{\rm EM}+\tau_l+\rho_l \ . \tag{49}$$

Here we used the fact that the potentials $V_{\rm VP}$ and V_{C2} are weak, so their phase shifts τ_l and ρ_l can simply be added to get the phase shift of $V_{\rm EMC}$.

We employ the same mechanism for partial waves with coupled channels. We therefore have to translate the addition law [Eq. (47)] for phase shifts into a multiplication law for S matrices. For this we use

$$S_{C+{\rm EMC}+N}^C=(S_{C+{\rm EMC}}^C)^{1/2}S_{C+{\rm EMC}+N}^{C+{\rm EMC}}(S_{C+{\rm EMC}}^C)^{1/2} \ . \tag{50}$$

The two matrices $S_{C+{\rm EMC}+N}^C$ and $S_{C+{\rm EMC}}^C$ can be defined by Eqs. (29) and (30) and are symmetric and unitary. Equation (50) defines $S_{C+{\rm EMC}+N}^{C+{\rm EMC}}$ also denoted as $S^{\rm EM}$ and called the nuclear-electromagnetic S matrix. By construction it is also unitary and symmetric. We need here the square root of a symmetric S matrix, which is related to a real and symmetric K matrix. One can explicitly define

$$S^{1/2}=(1+K^2)^{1/2}(1-iK)^{-1} \ , \tag{51}$$

where the first factor, the square root of a positive definite matrix, is uniquely defined.

The nuclear-electromagnetic S matrix can also be defined by matching the wave function to electromagnetic wave functions. This means that one can apply Eqs. (29) and (30) with the matrix solutions F and G replaced by $\bar{F}$ and $\bar{G}$, a regular and irregular solution for the potential $V_C+V_{\rm EMC}$. $\bar{F}$ and $\bar{G}$ can be defined very concisely by demanding them to be real and to satisfy

$$\bar{F}-i\bar{G}\underset{r\to\infty}{\sim}(F-iG)(S_{C+{\rm EMC}}^C)^{1/2} \ . \tag{52}$$

Since $S^{\rm EM}$ is symmetric and unitary we apply Eq. (43) to decompose it into nuclear-electromagnetic phase shifts.

We now look at the case of our model, where $V_{\rm EMC}$ is spin independent, so $S_{C+{\rm EMC}}^C$ is diagonal. Equation (50) then implies for the phase shifts

$$\delta_{lJ}=\delta_{lJ}^{\rm EM}+(\delta_{C+{\rm EMC}}^C)_l=\delta_{lJ}^{\rm EM}+\tau_l+\rho_l \ , \tag{53}$$

$$\epsilon_J=\epsilon_J^{\rm EM} \ . \tag{54}$$

Here the δ_{lJ} and ϵ_J are found decomposing $S_{C+{\rm EMC}+N}^C$, the total S matrix which was termed S above. Since Eq. (50) is also valid for uncoupled channels, we can substitute it for the S matrix in Eq. (44). This equation can then be rewritten as

$$M=M_C+M_{\rm EMC}+M_N \ , \tag{55}$$

where

$$\langle s,m'\,|\,M_{\rm EMC}(\theta)\,|\,s,m\rangle = \delta_{m'm}[f_{\rm EMC}(\theta)+(-1)^s f_{\rm EMC}(\pi-\theta)] \ , \tag{56}$$

with

$$f_{\rm EMC}(\theta)=\sum_{l=0}^{\infty}e^{2i\sigma_l}\frac{e^{2i(\delta_{C+{\rm EMC}}^C)_l}-1}{2ik}(2l+1)P_l(\theta) \ , \tag{57}$$

and

$$\langle s,m' \mid M_N(\theta,\phi) \mid s,m \rangle = 2 \sum_{\substack{l',J,l \\ s+l \text{ even}}} Y^{l'}_{m-m'}(\theta,\phi) C^{l\ s\ J}_{m-m'\ m'\ m} i^{l-l'} e^{i(\sigma_{l'}+\tau_{l'}+\rho_{l'})} \frac{\langle l',s \mid S_J^{\mathrm{EM}}-1 \mid l,s \rangle}{2ik} e^{i(\sigma_l+\tau_l+\rho_l)} \times C^{l\ s\ J}_{0\ m\ m} \sqrt{4\pi(2l+1)} \ . \tag{58}$$

In a phase shift analysis, the splitting of Eq. (55) is useful. The reason is that the first two terms are fixed and only have to be computed once. Only the summation of Eq. (58) for the nuclear part of the amplitude has to be repeated many times in the fitting process, and this summation converges much more rapidly than Eq. (44), because the nuclear interaction is of much shorter range than the electromagnetic forces. In our energy range it is sufficient to use only terms up to $J=10$. The slowly converging part, which is still present in Eq. (57), needs several hundreds of terms.

Finally we mention another type of phase shift that is frequently used. It is denoted by δ^C and can be defined, using our full notation, as $\delta^C=(\delta^C_{C+N})_l$. Within a potential model these phase shifts can be obtained by removing the (very long range) V_{EMC} from the model, so they are much easier to compute. Another advantage is that an effective range formula for δ^C is much simpler than those for other types. Unfortunately, the definition of δ^C is model dependent. The difference between the ordinary δ and δ^C can be given in distorted-wave Born approximation

$$\delta_l-\delta_l^C=(\delta^C_{C+\mathrm{EMC}+N})_l-(\delta^C_{C+N})_l \approx -\frac{M_p}{k}\int_0^\infty dr\, \chi_l(r) V_{\mathrm{EMC}}(r) \chi_l(r) \ , \tag{59}$$

where χ_l is the wave function for the potential V_C+V_N. The case where V_{EMC} contains only the vacuum polarization potential was first treated by Foldy and Eriksen.[66] In that case the phase shift difference in Eq. (59) is termed the Foldy correction

$$\Delta_l=(\delta^C_{C+\mathrm{VP}+N})_l-(\delta^C_{C+N})_l \approx -\frac{M_p}{k}\int_0^\infty dr\, \chi_l^2(r) V_{\mathrm{VP}}(r) \ . \tag{60}$$

In our case V_{EMC} also contains V_{C2} of the improved Coulomb potential [Eq. (25)]. Therefore we define an improved Coulomb-Foldy correction $\tilde{\Delta}_l$ by

$$\tilde{\Delta}_l=(\delta^C_{C+\mathrm{VP}+N})_l-(\delta^C_{C+N})_l \approx -\frac{M_p}{k}\int_0^\infty dr\, \chi_l(r)[V_{\mathrm{VP}}(r)+V_{C2}(r)]\chi_l(r) \ . \tag{61}$$

Δ_l and $\tilde{\Delta}_l$ are in principle model-dependent quantities, depending on the nuclear interaction, via the wave function $\chi_l(r)$. For the higher partial waves that are at low energies only weakly affected by the nuclear interaction, one can approximate $\chi_l(r)$ by the regular Coulomb function. In practice this suffices for all partial waves except the $^1S_0$. For $l \geq 1$, Eq. (59) therefore reduces to the CDWBA for the phase shifts $\delta^C_{C+\mathrm{EMC}}$ and we have

$$\Delta_l=\tau_l, \quad l \geq 1 \qquad \tilde{\Delta}_l=\tau_l+\rho_l, \quad l \geq 1 \ . \tag{62}$$

Hence the phase shifts of type δ^C for $l \geq 1$ are practically equal to the nuclear-electromagnetic phase shifts δ^{EM} of Eq. (49). This also applies to the coupled channels case [Eq. (54)].

Only for the $^1S_0$ one has to do better, the correct χ_l has to be used in Eq. (59). Noyes and Lipinski[11] give Δ_0 for three (simple) potential models. We have computed Δ_0 up to 30 MeV for two modern NN potentials: the Nijmegen (N78) (Ref. 27) and the Paris (P80) (Ref. 28) potential. The values never differ more than 10^{-3} deg between these models, except for model (c) of Ref. 11, which consists of OPE plus a purely attractive Bargmann potential. Since this is smaller than the accuracy with which the $^1S_0$ phase shift is determined at any energy (Sec. VI C), we believe that these corrections are sufficiently model independent for a wide range of nuclear interaction models. If one wants to treat the electromagnetic interaction better, the next step in improvement would be taking into account the spatial extension of the charges.[67] This would give rise to a further improved Foldy correction.

The values obtained with the Nijmegen (N78) (Ref. 27) potential for Δ_0 and $\tilde{\Delta}_0$ are given in Table V. There one also finds the vacuum polarization phase shift τ_l and the phase shift ρ_l of V_{C2}. With these quantities any other type of phase shift can be translated to a standard phase shift δ_l as defined in Sec. IV A.

We believe that the results of an analysis should preferably be given as phase shifts of this latter type, δ_l or $(\delta^C_{C+\mathrm{EMC}+N})_l$, because they are most directly related to the asymptotic wave function. The definition of the other types is model dependent. Only the δ^E of Eq. (49) could in principle be used, but the symbol δ^E has also been used to denote other kinds of phase shifts.[12,17] Therefore we always use the δ_l type to give our results.

V. DATA ANALYSIS

A. Statistical considerations

1. *The procedure*

In any kind of fitting one compares the predictions of a certain model with the experimental data and then adjusts the parameters of this model to obtain the best agreement. In our analysis we are mainly interested in extracting values for the phase shifts and the pion-coupling constant from the data. We employ the *P*-

matrix model (Sec. II) to describe the phase shifts as energy-dependent quantities. We make use of three kinds of fitting.

(1) In a multienergy (me) fit, all parameters of our model are fitted to all data of our selected data set in the entire energy range.

(2) In a single-group fit only data of one experiment are used. Only 1 or 2 phase shifts at the energy of the experiment (or at some central energy if the data within this group have been taken at different energies) serve as parameters. Other phase shifts and, if necessary, the energy dependence of the phase shifts searched for, are fixed using me results. The purpose of single-group fits is to judge the quality of each group in the determination of the phase shifts. These single-group phase shifts can show friction between groups. They can also serve as a means to detect systematic errors that have not been specified in the data publication. In Sec. V A 5 we will give an example of such a situation.

(3) In a single-energy (se) fit, the subset of data with energies close to some central value is used. The phase shifts one wants to search for at these energies act as parameters. Their proper energy dependence has to be preserved using me results.

Since the energy dependence of the phase shifts produced by the model is not so important in se fits, se fits are less model dependent and can be used to judge the me parametrization. Furthermore, se fits are more likely to satisfy the conditions for a least-squares fit [see Sec. V A 3 condition (ii)]. Therefore, the values for the phase shifts with error matrices resulting from se fits are the most reliable, model-independent description of the data in terms of phase shifts. They can be used to judge a model of the interaction or to adjust its parameters to the data. The advantage of a me fit over a se fit is that it averages the statistical fluctuations at different energies. In all three kinds of fits the method of least squares has been used, which will be described below.

2. *Least-squares fit*

We consider the case of a data set consisting of several groups of measurements. A group is a set of measurements obtained from one experiment. The measurements within a group usually have a common normalization uncertainty and there may also be other systematic errors. We denote the N_A measurements and errors within a group A by $E_{A,i}\pm\epsilon_{A,i}$ $(i=1,\ldots,N_A)$. Suppose for a moment that no groups contain specified systematic errors, such as normalization uncertainties. The model values for the scattering observables we call $M_{A,i}(\mathbf{p})$. They depend on the model parameters p_α $(\alpha=1,\ldots,N_{\text{par}})$. The agreement between theory and experiment can then be seen in χ^2

$$\chi^2(\mathbf{p})=\sum_A \chi^2_A(\mathbf{p}) =\sum_A \sum_{i=1}^{N_A}\left[\frac{M_{A,i}(\mathbf{p})-E_{A,i}}{\epsilon_{A,i}}\right]^2 . \tag{63}$$

A least-squares fit now means that Eq. (63) has to be minimized with respect to all parameters p_α. The obtained parameter values are the predictions we get from the data. The error matrix E for these parameters is related to the second derivative of χ^2, evaluated at $\chi^2_{\min}$, the minimum of χ^2 with respect to all parameters

$$(E^{-1})_{\alpha\beta}=\frac{1}{2}\frac{d^2\chi^2(\mathbf{p})}{dp_\alpha dp_\beta}\bigg|_{\mathbf{p}=\mathbf{p}_{\min}} \tag{64}$$

From the error matrix E one defines the one standard deviation (s.d.) error for parameter p_α as $(E_{\alpha\alpha})^{1/2}$. By approximating χ^2 as a quadratic function near its minimum, one can show that

$$(E_{\alpha\alpha})^{-1}=\left[\frac{1}{2}\frac{d^2}{dp_\alpha^2}\min_{\substack{p_\beta\\ \beta\neq\alpha}}\chi^2(\mathbf{p})\right]\Bigg|_{p_\alpha=(\mathbf{p}_{\min})_\alpha} \tag{65}$$

This means that the error $(E_{\alpha\alpha})^{1/2}$ is the maximum deviation possible in p_α without raising χ^2 by more than 1, while other parameters are allowed to vary. Equation (65) is valid also if α stands for a subset of the parameters. Then $E_{\alpha\alpha}$ is the error matrix, truncated to this subset of parameters. We make use of this to define χ^2 when, as usual, groups of data have an overall (multiplicative) norm uncertainty. Such a normalization has to be introduced as a normalization parameter ν_A, for which the experimentalist states $\nu_A=1\pm\epsilon_{A,0}$. This would lead to a χ^2 depending on many more parameters. Since we are usually interested in determining the model parameters only, we avoid this by defining

$$\chi^2(\mathbf{p})=\sum_A \chi^2_A(\mathbf{p}) =\sum_A \min_{\nu_A}\sum_{i=1}^{N_A}\left[\frac{\nu_A M_{A,i}(\mathbf{p})-E_{A,i}}{\epsilon_{A,i}}\right]^2+\left[\frac{\nu_A-1}{\epsilon_{A,0}}\right]^2 , \tag{66}$$

where $\mathbf{p}$ contains only the model parameters. The use of this χ^2 in Eq. (64) immediately gives the error matrix, restricted to the model parameters. For calculations, the χ^2 of Eq. (66) is very useful. The minimum with respect to the normalization parameters ν_A can be found trivially by minimizing a quadratic function. Therefore one can easily compute $\chi^2(\mathbf{p})$ of Eq. (66) with the ν_A adjusted implicitly. So the function to be minimized iteratively, depends only on the model parameters. For the groups where ν_A is entirely unknown ($\epsilon_{A,0}=\infty$), the second squared term in Eq. (66) is absent. If ν_A is exactly known ($\epsilon_{A,0}=0$), ν_A is fixed to 1 and the second squared term is again absent. Some groups[3] have, apart from ν_A, some more specified systematic errors, given as normalization parameters with different angle-dependent influences. These more complicated systematic errors can be treated analogously.

Since the first derivative of χ^2 with respect to all parameters is zero in the minimum, the second derivative matrix $S=2E^{-1}$ together with the minimum value of χ^2 ($\chi^2_{\min}$) can serve as an approximation for $\chi^2(\mathbf{p})$ in the neighborhood of the minimum. In the case of our se fits,

where the parameters are phase shifts, this allows the computation of χ^2 for any model that produces phase shifts. Fitting the parameters of such a model to our se values and error matrices has several advantages. First of all, one does not have to compute model values for every measured observable. Also the detailed analysis and selection of the data is avoided. Finally, the obtained χ^2 can be compared with the value we reach in our me fit. Our se minima of χ^2 show the minimum values that are attainable.

It is better not to compare phase shifts with our results by using only the errors computed from the diagonal elements of our error matrix, because phase shifts that seem to be in reasonable accordance with ours (when this accordance is measured in terms of these errors) can still be very bad, due to the correlation between the phase shifts.

3. *Conditions for a least-squares fit*

In order to get meaningful results from a least-squares fit some conditions must be satisfied.

(i) The model should be able to give (almost) the true values of the observables for some values of the parameters. This could be called the true values of the parameters.

(ii) The model predictions $M_{A,i}(\mathbf{p})$ should be approximately linear as a function of the parameters in the parameter region where $\chi^2-\chi^2_{\min}\lesssim 1$.

(iii) The measurements have to be free from unspecified systematic errors (unbiased), and their statistical errors should be specified correctly. Stated differently, each measurement should have a probability distribution function, which has as its expectation value the true value of the observable, and as its variance (mean-square deviation from the expectation value) the $\epsilon^2_{A,i}$. The shape of the probability distribution function may be arbitrary, as long as the variance exists.

If these conditions are met, one can derive some desired properties for the parameters obtained in the fit. The least-squares fit is viewed then as a method (estimator) to derive parameters as a function of the input measurements. Since the latter are stochastic variables, the same is valid for the parameters. These parameters will now have as their expectation values precisely the true values mentioned above. So the least-squares method provides an unbiased estimate for the parameters. Furthermore, the variance matrix of these parameters is precisely the matrix E defined by Eq. (64), which is the justification for calling this the error matrix. If the measurements have Gaussian probability distribution functions, one obtains for the parameters a probability distribution function that is also Gaussian (multivariate normal distribution). If the data have arbitrary probability distribution functions, then, due to the central-limit theorem of statistics, one still obtains a Gaussian probability distribution function for the parameters in the limit of a large number of data.

We now return to the three conditions. As stated above, we would like to satisfy them especially in se fits, in order to get a reliable representation of the χ^2 hypersurface. In these analyses only a limited number of phase shifts can be used as parameters. To satisfy condition (i) the phase shifts not searched for (higher l phases) have to be fixed at the correct values. Therefore an important quantity with respect to this condition is M_{EMC}, the long-range amplitude of Eqs. (56) and (57). If one disregards some small contribution to M_{EMC} or to the higher l phase shifts, this can still result in a good fit, but the fitted phase shifts will be biased. An example of such a situation can be seen in older analyses that neglect vacuum polarization for orbital angular momentum $l>0$. This error is compensated roughly by changing the central P-wave phase shift combination Δ_C.[26]

One can see that condition (ii) is easily satisfied, since the parameter region involved is typically much less than a degree in each phase shift.

If condition (iii) is violated by some measurements, it will often be necessary to reject them, in order to obtain reliable results. We will now describe some means to detect such data.

4. *Expectations for χ^2*

In a least-squares fit to data as described above, we have to define the following numbers. The number of data N_{dat} consists of the N_{obs} measured scattering observables and the N_{ne} normalization parameters for which an error is given: $N_{\mathrm{dat}}=N_{\mathrm{obs}}+N_{\mathrm{ne}}$. Thus N_{dat} is the number of squared terms in Eq. (66). The total number of parameters N_{fp} used to minimize χ^2 [Eq. (66)] includes the N_{par} model parameters plus the N_{n} fitted normalization parameters: $N_{\mathrm{fp}}=N_{\mathrm{par}}+N_{\mathrm{n}}$. So $N_{\mathrm{n}}-N_{\mathrm{ne}}$ is the number of unbounded normalization parameters, which will be equal to the number of groups of relative measurements. The number of degrees of freedom N_{df} is given by the difference between the number of data and the number of parameters: $N_{\mathrm{df}}=N_{\mathrm{dat}}-N_{\mathrm{fp}}$.

If the conditions for a least-squares fit are fulfilled, one can show that the obtained minimum χ^2 has the expectation value $\langle\chi^2_{\min}\rangle=N_{\mathrm{df}}$. However, the uncertainty in this prediction depends on the shape of the probability distribution functions of the individual measurements. In the following we will assume, if necessary, that these are Gaussian. In the Appendix this assumption is tested and there it is shown that the χ^2 distribution of the experiments agrees very well with the expectation for Gaussian data. For scattering data one certainly expects this, because the Gaussian is the limiting form for large numbers of the Poisson distribution that would emerge from event counting. With this assumption one can assign a probability distribution function to $\chi^2_{\min}$

$$P(\chi^2_{\min})=P_{N_{\mathrm{df}}}(\chi^2_{\min})\ , \tag{67}$$

where

$$P_\nu(t)=\frac{1}{\Gamma(\nu/2)2^{\nu/2}}t^{(\nu/2)-1}e^{-t/2} \tag{68}$$

is the χ^2 distribution for ν degrees of freedom. It has expectation value ν and variance 2ν. This leads for $\chi^2_{\min}$ to

the expectation value

$$\langle \chi^2_{\min} \rangle = N_{\mathrm{df}} \pm \sqrt{2N_{\mathrm{df}}} \ . \tag{69}$$

One often defines the χ^2 per degree of freedom χ^2/N_{df} or M value for which one expects

$$\langle \chi^2/N_{\mathrm{df}} \rangle = 1 \pm \sqrt{2/N_{\mathrm{df}}} \ . \tag{70}$$

We now look at the contribution to χ^2 of one data point, denoted by $\chi^2_{A,i}$. This is one individual term in χ^2 of Eq. (66). For a moment, assume that no normalization parameters have to be fitted and that the model has no parameters (or all parameters are fixed at their true values). The assumption of Gaussian measurements then gives us for each squared term in χ^2 a probability distribution function $P_1(\chi^2_{A,i})$ of Eq. (68). Since this probability distribution function has expectation value 1, the expectation value of the total χ^2 will be the number of these squared terms. In the case where N_{par} model parameters and N_{n} normalization parameters are fitted, we know that the N_{dat} terms lead to an expectation value N_{df}. Therefore it seems reasonable to assume that a somewhat narrower probability distribution function for each term results, due to the fitting of these parameters, e.g.,

$$P(\chi^2_{A,i}) = \alpha^{-1} P_1(\alpha^{-1}\chi^2_{A,i}) \ , \tag{71}$$

with $\alpha = N_{\mathrm{df}}/N_{\mathrm{dat}}$. In our final me fit $\alpha = \frac{343}{389}$. In the Appendix this probability distribution function is compared with the experimental distribution of our final fit, and an excellent agreement is found.

One can also look at the χ^2 contribution of a group within a large data set. Again we start assuming that there are no model parameters. A group of N_A measurements with a fixed normalization will then have for its contribution to χ^2, χ^2_A, a χ^2 distribution for N_A degrees of freedom. For a group of relative measurements this reduces to $N_A - 1$ degrees of freedom after the normalization is fitted. If a group contains a normalization datum ($\nu_A = 1 \pm \epsilon_{A,0}$), it actually consists of $N_A + 1$ data, but after the norm is fitted, the probability distribution function for its contribution to χ^2 will again be a χ^2 distribution for N_A degrees of freedom. Adding the expectation values of all groups, we now reach $N_{\mathrm{obs}} - (N_{\mathrm{n}} - N_{\mathrm{ne}})$ as the expectation value of the total χ^2. If model parameters are fitted, this has to be reduced to the expected N_{df}. We again assume that the distributions for each group are narrowed, due to the fitting of the model parameters

$$P_{\mathrm{group}}(\chi^2_A) = \beta^{-1} P_{N'_A}(\beta^{-1}\chi^2_A) \ , \tag{72}$$

with $N'_A = N_A - 1$ for groups of relative measurements, and $N'_A = N_A$ otherwise. In both cases $\beta = N_{\mathrm{df}}/(N_{\mathrm{df}} + N_{\mathrm{par}})$. In our final me fit $\beta = \frac{343}{355}$.

Serious deviations from the behavior expressed in Eqs. (67), (71), and (72) are an indication that the conditions for a least-squares fit are violated. Therefore the above probability distribution functions can be used to construct rejection criteria.

5. *Rejection criteria*

There are two ways in which a measurement can fail to satisfy condition (iii) of Sec. V A 3. The errors $\epsilon_{A,i}$ could be specified incorrectly (too small or too large), or there may be systematic errors present. If the errors are overestimated, there is of course no reason to reject these data. In the case of too-small errors, the data pretend to give more information than they actually do, which can lead to erroneous results. Systematic errors are errors that are in some way correlated for all measurements within a group. If they are specified clearly, systematic errors can be dealt with, as in the case of normalization errors. Often this is not the case, and statistical and systematic errors are somehow combined to so-called total errors. The following example shows how systematic errors can lead to wrong results.

Suppose that in a group of N measurements of the same quantity the error is purely systematic. This means that N times the result $T + S$ is obtained, where T is the true value. The experimentalist does not know S, but he has only some expectation value for it, say $\bar{S}$. Each measurement now has the total error $\epsilon_i = \bar{S}$. A least-squares fit to determine T would result in the value $T + S$, with error $\bar{S}/\sqrt{N}$, which is not correct. Of course in this case the systematic nature of the errors is clearly visible. As a more general example we look at a group of N measurements of an angle-dependent observable at a number of angles. Again we assume that the errors are purely systematic and again the number S is a measure for the magnitude of the systematic errors. The measurements result in $E_i = T_i + S f_i$, where the f_i allow for an angle-dependent systematic error and are normalized such that $\sum f_i^2 = N$. The experimentalist gives for each measurement an error $\epsilon_i = \bar{S}$, the estimated magnitude of S. If this group is analyzed in a single-group fit, it is possible that a fitted parameter p_α can compensate for the effect of S. In that case a $\chi^2 \ll N_{\mathrm{df}}$ will be obtained. So it appears that a systematic error can sometimes be detected from a very low χ^2 in a single-group fit. One will also get a value for the parameter p_α with a deviation from the true value proportional to S, independent of N. The fit, however, will give an estimate for the accuracy of this parameter that is proportional to $\bar{S}/\sqrt{N}$. The group pretends to determine this parameter more accurately than is actually the case.

If the same group is analyzed in a me fit as part of a large data set, it might be detected in another way. Let us assume that the parameters are practically fixed to the true values by the rest of the data set. Then the χ^2_A of the group in question will not have the usual probability distribution function of Eq. (72), since only one single parameter S is responsible for its errors. If one assigns a Gaussian probability distribution function to S one can show that the probability distribution function for χ^2_A will be $N^{-1} P_1(\chi^2_A/N)$. In any case we expect a probability distribution function which is not as sharply peaked around N, so very high and very low values of χ^2_A are more likely to occur. Therefore they can serve as an indication for systematic errors.

Finally we mention the problem of outliers, individual

data points with a very high $\chi^2_{A,i}$. These can be viewed as resulting from a faint, but very broad background added to the probability distribution function of the data. It can be shown that if a background exists, rejection of outliers will lead to more accurate values for the parameters (having smaller variance). Different methods exist to reject outliers. We use the 3σ criterium, as explained below.

In this analysis we reject groups of measurements if there is strong evidence against them. Only conditions that would have a very small chance to occur for a correct data set serve as rejection criteria.

We now list our rejection criteria.

(1) Any measurement $E_{A,i}$ with $\chi^2_{A,i} > 9$ is rejected as an outlier. This corresponds to the 3σ criterium, since a $\chi^2_{A,i}$ of 9 means a misfit of three times the experimental error. For Gaussian data and a parameter-free model there would be a chance of only 0.27% for a measurement to be rejected. Due to the effect of fitting, we expect an even smaller chance; Eq. (71) leads to 0.14%.

(2) To reject data with systematic errors, we leave out groups of which the single-group fit disagrees too much with the me fit. We use an analogy of the 3σ criterium. The group is rejected if the parameter values in the me and single-group fits show a difference of more than three times the accuracy with which this parameter is determined in the single-group fit. In the case of a one-parameter single-group fit χ^2_A is not allowed to drop by more than 9 below χ^2_A of this group in the me fit. For an n parameter single-group fit, this is generalized to a maximum χ^2_A drop by $\chi^2_{\text{high}}(n)$ of Table II. This criterium is tailored in such a way that the chance that a group of correct Gaussian data will be rejected is 0.27% if the effect of fitting the me parameters is neglected. In fact also here the chance is even smaller.

(3) As another means against systematic errors, a group is rejected if its χ^2_A is less than $\chi^2_{\text{low}}(N_{\text{df}})$ in a single-group fit with N_{df} degrees of freedom. The values of χ^2_{low}, listed in Table II, are calculated to give again a chance of 0.27% for a correct group to be rejected. A group is also rejected, if its me χ^2_A is already too low. We do not use this criterium if $N_{\text{df}} \leq 3$, because then a small χ^2_A is no longer highly improbable.

(4) Finally we leave out a group of its χ^2_A in the me fit exceeds $\beta\chi^2_{\text{high}}(N_A)$, where β is as specified below Eq. (72). From Eq. (72) it can be seen that this gives again the 0.27% chance to reject correct data. For a group of N_A relative measurements, the upper limit becomes $\beta\chi^2_{\text{high}}(N_A - 1)$.

By construction of all these criteria should almost never come into action in the case of correct data. If they do reject a considerable fraction of the data set, one should be suspicious, because those criteria that reject data for their high contribution to χ^2 can also indicate that the model does not have enough freedom. In this analysis the only sets of data rejected for their large contribution to χ^2 consist of the 50 Berkeley68 (Ref. 68) cross sections (all rejected data are discussed in Sec. V B). In that case, however, there are enough comparable measurements, and therefore one can see that the Berkeley68 data clearly contradict the other data (see also Ref. 12). Therefore it is very likely that something is wrong with these data.

The criteria are meant to avoid unwanted effects, like systematic errors and underestimated errors, because they can lead to less accuracy in the parameters than the obtained error matrix suggests. Instead of rejecting data, this might also be remedied by enlarging by hand the errors of suspect measurements. With which factor the errors should be enlarged would have to be guessed from the amount of systematic error one sees in the data. Incorporating data with enlarged errors has the disadvantage that the above expectations for χ^2 (e.g., $\chi^2/N_{\text{df}} = 1 \pm \sqrt{2/N_{\text{df}}}$) are not valid anymore. The Wisconsin66 1–3 MeV cross-section data[69] form an example of the above situation. Before the publication of the Zürich78 data,[3] the Wisconsin66 data were the only cross sections below 5 MeV and away from the interference minimum that were incorporated in analyses. The errors, however, contained a large systematic component. Therefore, before 1978 one could not reject the Wisconsin66 data without throwing away valuable information, but one should have enlarged the errors. Presently the importance of the Wisconsin66 data has faded, since one has the Zürich78 data.[3] Therefore we do not include the Wisconsin66 data in our data set. The Wisconsin66 data are not in disagreement with our multienergy fit, since they give $\chi^2 \approx 15$ (for 50 data).

B. The data

The latest 0–30 MeV pp analysis[1,2] incorporated 253 measurements. Since then a lot of new data have been published. An analysis of all 0–3 MeV data has been performed recently by van der Sanden, Emmen, and de Swart.[17] At these very low energies only differential cross-section data are available. Earlier analyses had only available the 5 Los Alamos64 data[70] around the interference minimum, measured by Brolley *et al.*, and the 51 Wisconsin66 1–3 MeV data[69] of Knecht, Dahl, and Messelt. The 9 Basel73 data[4,5] below 2 MeV have not been included in the earlier analyses. It has been known for a long time that the Wisconsin66 data have errors with a large systematic component (see also van der Sanden, Emmen, and de Swart[17] or SSH[12]). In SSH[12] a normalization error can be found which incorporates systematic errors that are constant with angle. However, a

TABLE II. Values of χ^2 used in the rejection criteria (see text).

n	1	2	3	4	5	7	10	15	20	25	30
$\chi^2_{\text{high}}(n)$	9.0	11.8	14.2	16.3	18.2	22	27	35	42	49	56
$\chi^2_{\text{low}}(n)$				0.15	0.31	0.81	1.8	4.1	6.8	9.8	13

large systematic component remains, as the bulk of the systematic errors were angle dependent. Therefore the publication of the 174 Zürich78 differential cross-section data below 1 MeV by Thomann, Benn, and Münch[3] meant a tremendous addition to the very-low-energy data.

At about 5 and 10 MeV Barker *et al.* recently reported the 26 Wisconsin82 high-precision analyzing power (polarization) data.[6,7] Bittner and Kretschmer[9] published 6 Erlangen82 analyzing power data at about 6 MeV. An Erlangen80 measurement of the spin-correlation parameter A_{yy} (C_{NN}) at about 10 MeV was published by Obermeyer *et al.*[10] Another addition to the data is formed by the 13 Los Alamos76 cross sections around 20 MeV measured by Jarmie and Jett.[8]

Most of the low-energy data are differential cross-section data. Such data primarily determine the $^1S_0$ phase shift and the central combination of P-wave phase shifts Δ_C. The importance of polarization measurements lies in the fact that they allow a determination of the tensor and spin-orbit combinations of P-wave phase shifts Δ_T and Δ_{LS}. Therefore especially the Wisconsin82 (Refs. 6 and 7) data, that are much more precise than the older Wisconsin75 (Ref. 71) data, mean an important addition to the low-energy data. The above-mentioned P-wave combinations are defined in Eq. (19).

Our initial set of data consisted of all pp scattering measurements for $T_{lab} \lesssim 30$ MeV published in a regular physics journal after approximately 1955 (because of the relative precision of the newer measurements). A detailed list of the major part of the data can be found in the Nucleon-Nucleon Scattering Data Tables of Bystricky and Lehar.[72,73]

Unfortunately enough, there exists a lot of data[29–33] that have not been published or that have only been reported in conference proceedings. We believe it is a good policy to omit unpublished data in an analysis, although we realize that much effort has been made to take these measurements and that perhaps nothing is wrong with these data, except that they lack the detailed scrutiny they would have had when prepared for a formal publication. These unpublished data are 117 Minnesota77 differential cross-section measurements of Hegland *et al.*[29,30] from 6 to 20 MeV, 9 Los Alamos76 analyzing power data at 16 MeV of Lovoi *et al.*[31,32] and, somewhat less recent, 8 Grenoble70 polarizations at 30 MeV of Arvieux *et al.*[33] The new Erlangen86 analyzing power data at 12 MeV of Kretschmer *et al.*[74] had only appeared in a conference proceeding before this analysis was finished and are therefore not included. We find that there is friction between these data[74] and the Wisconsin82 (Refs. 6 and 7) data.

Had we included the unpublished data, our results surely would have changed. Apart from the fact that with the Los Alamos76 analyzing power data one can give se phase shifts at 16 MeV, the most important change in our results would arise from the inclusion of the Minnesota77 $d\sigma/d\Omega$ data. Of these, the group at 13.6 MeV would not have survived our rejection criteria, but the remaining 100 data are almost as restrictive to the phase shifts as the 124 $d\sigma/d\Omega$ measurements we have in our final data set (see below) between 5 and 20 MeV. Therefore in the discussion of the results (Sec. VI A) we will describe the changes in the results that would arise from inclusion of the Minnesota77 and Los Alamos76 data.

A list of all groups of published data is given in the data reference table, Table III. As the 0–3 MeV data have been analyzed recently by van der Sanden, Emmen, and de Swart[17] we accept of their results the rejection of the Basel73 (Refs. 4 and 5) and the Wisconsin66 (Ref. 69) data.

As a first step, the values of our 10 P-matrix parameters for the lower partial waves [Eqs. (16), (20), (21), and (23)] are adjusted to this initial set of data (fit 1), where we keep the remaining parameters of the model fixed at the reasonable values: $g^2_{pp\pi^0}/4\pi = 14.4$ and $b = 1.8$ fm.

The 16 old Berkeley67 polarization data[76] between 10 and 20 MeV, the 17 Berkeley68 differential cross sections[68] at 9.918 MeV, 3 differential cross-section data points from different groups,[70,85,78] and 1 normalization datum[78] appear to be inconsistent (criteria 4 and 1 of Sec. V A 5) with fit 1 and are therefore rejected. None of these rejections is surprising, compared with other analyses, except perhaps the rejection of the normalization datum of the Los Alamos70 (Ref. 78) differential cross sections at 9.69 MeV. The Los Alamos70 cross sections[78] at 9.69 and 9.918 MeV are the reanalyzed data of an earlier publication.[79] The reanalysis of the data was done, since the phase shift analysis of Holdeman, Signell, and Sher[94] showed discrepancies in the data around 10 MeV. The reanalyzed data[79] are about 2% larger than the original. For the 9.918 MeV data this new normalization is in accordance with our results. For the 9.69 MeV data we find a norm of 0.9826, about 2% less. Naisse[2] finds about the same normalization, but he enlarges the normalization error artificially, since in his analysis[2] the 9.69 MeV data of Los Alamos70 (Ref. 78) and Minnesota59a (Ref. 77) are treated as one group with a common normalization datum.

In the second step, the 10 P-matrix parameters are tuned (fit 2) to fit the remaining (i.e., initial minus rejected) data. Since fit 2 already results in $\chi^2/N_{df} < 1$, we accept fit 2 as having determined the phase shifts well enough to serve in the single-group analyses. In these single-group analyses, we adjust the important phase shifts to fit one group of data. The important phase shifts are the ones that are best determined by the specific type of experiment. For differential cross sections we fit $\delta(^1S_0)$ and Δ_C, for other types of observables we fit Δ_T and Δ_{LS}, if possible. All other phase shifts are preserved at the fit-2 values. For groups consisting of data at different energies, we want to vary at these energies an important phase shift with only one parameter. Therefore we fit a constant to be added to the energy-dependent P matrix of fit 2. For low energies this procedure is better than fitting a constant to be added to the phase shift, since it ensures the proper threshold behavior.

These single-group analyses result in the χ^2 values and values and errors for the important phase shifts in the columns labeled χ^2_{sg} and sg phases of the data reference

TABLE III. Data reference table. me = multienergy, sg = single group. All phase shifts tabulated are with respect to Coulomb functions in degrees (from the bar decomposition of the total S matrix).

T_{lab} (MeV)	Institute, Reference	Number, Type of data[a]	% norm error	Deleted data	Predicted norm[b]	χ^2_{me}	χ^2_{sg}	sg phases	me phases	Comments
0.337 66, . . . , 0.405 17	Los Alamos64 70	5σ	∞	0.372 83 MeV	1.0162	3.79	3.52	$^1S_0 = 14.5127 \pm 0.0068$ at 0.382 54 MeV	14.5096	d
0.350 03, . . . , 0.420 03	Zürich78 3	36σ	∞		0.9976	38.79	38.76	$^1S_0 = 14.5100 \pm 0.0033$ at 0.382 54 MeV	14.5096	c
0.350 09	Zürich78 3	17σ	0.16		0.9993	25.18	25.06	$^1S_0 = 13.190 \pm 0.027$	13.199	c,e
0.400 04	Zürich78 3	3σ	0.21		1.0009	1.05	0.88	$^1S_0 = 15.26 \pm 0.14$	15.20	
0.420 06	Zürich78 3	22σ	0.16		0.9993	38.06	37.88	$^1S_0 = 15.987 \pm 0.025$	15.976	c,e
0.499 23	Zürich78 3	39σ	0.16		0.9990	31.78	28.18	$^1S_0 = 18.8916 \pm 0.0060$ $\Delta_C = -0.0600 \pm 0.0039$	18.8979 −0.0558	c
0.499 25	Basel73 4,5	3σ	0.03	all						f
0.749 96	Zürich78 3	26σ	0.16		0.9988	16.14	14.04	$^1S_0 = 26.691 \pm 0.011$ $\Delta_C = -0.0619 \pm 0.0042$	26.684 −0.0558	c
0.991 83	Zürich78 3	31σ	0.16		0.9989	25.45	22.12	$^1S_0 = 32.443 \pm 0.014$ $\Delta_C = -0.0580 \pm 0.0040$	32.418 −0.0561	c
0.991 9	Basel73 4,5	3σ	0.03	all						f
1.397, . . . , 3.037	Wisconsin66 69	51σ		all						f
1.880 6	Basel73 4,5	3σ	0.03	all						f
4.978	Kyoto75 75	17σ	0.4		1.0038	19.71	13.27	$^1S_0 = 54.49 \pm 0.11$ $\Delta_C = -0.020 \pm 0.016$	54.69 −0.053	
5.05	Wisconsin82 6,7	11P	1.0		1.0012	5.84	4.45	$\Delta_T = -0.426 \pm 0.017$ $\Delta_{LS} = 0.056 \pm 0.015$	−0.415 0.073	
6.141	Erlangen79 9	6P	0.0	all						h
6.141	Berkeley68 68	17σ	0.4	all						i,j
6.968	Kyoto75 75	17σ	0.4		1.0062	18.49	12.80	$^1S_0 = 55.33 \pm 0.11$ $\Delta_C = -0.004 \pm 0.015$	55.54 −0.027	

TABLE III. (*Continued*).

T_{lab} (MeV)	Institute, Reference	Number, Type of data[a]	% norm error	Deleted data	Predicted norm[b]	χ^2_{me}	χ^2_{sg}	sg phases	me phases	Comments
8.03	Kyoto75 75	17σ	0.4		1.0061	14.31	9.03	$^1S_0 = 55.31 \pm 0.12$ $\Delta_C = 0.016 \pm 0.015$	55.53 −0.005	
8.097	Berkeley68 68	16σ		all						i,j
9.57	Erlangen80 10	$1A_{yy}$	0.0		1.0	0.20	0.0	$\Delta_T = -0.82 \pm 0.25$	−0.91	
9.6, . . . , 19.7	Berkeley67 76	$16P$	0.0	all						g
9.69	Minnesota59a 77	26σ	0.73		0.9857	15.69	11.00	$^1S_0 = 55.51 \pm 0.20$ $\Delta_C = -0.017 \pm 0.030$	55.21 0.039	k,l
9.69	Los Alamos70 78,79	5σ	∞	norm.	0.9826	3.53	0.41	$^1S_0 = 55.6 \pm 3.0$ $\Delta_C = -0.045 \pm 0.070$	55.21 0.039	d
9.85	Wisconsin82 6,7	$15P$	1.0		0.9980	12.99	12.75	$\Delta_T = -0.9352 \pm 0.0090$ $\Delta_{LS} = 0.212 \pm 0.016$	−0.9335 0.205	
9.918	Berkeley68 68	17σ	0.4	all						i,d
9.918	Los Alamos70 78,79	10σ	0.37	20.05°	0.9956	15.26	6.39	$^1S_0 = 55.24 \pm 0.15$ $\Delta_C = -0.046 \pm 0.034$	55.14 0.046	d
10.0	Wisconsin75 71	$7P$	0.0		1.0	9.56	5.41	$\Delta_T = -0.862 \pm 0.049$ $\Delta_{LS} = 0.31 \pm 0.10$	−0.950 0.21	
11.4, . . . , 26.5	Saclay67 80	$4A_{xx}$ $4A_{yy}$	∞		1.0022	3.04	0.71	$\Delta_T = -1.917 \pm 0.044$ $\Delta_{LS} = 0.49 \pm 0.13$ at 19.15 MeV	−1.832 0.54	m
13.6	Los Alamos70b 78	11σ	0.33		1.0014	13.78	13.38	$^1S_0 = 53.70 \pm 0.13$ $\Delta_C = 0.151 \pm 0.042$	53.79 0.183	
14.16	Tokyo60 81	17σ	0.0	all						k,h
16.2	Princeton59 82	$1P$	0.0		1.0	0.68	0.0	$\Delta_{LS} = 2.8 \pm 1.5$	0.4	k
18.28	Princeton54 83	8σ	1.5		0.9880	5.20	3.49	$^1S_0 = 52.21 \pm 0.54$ $\Delta_C = 0.71 \pm 0.29$	51.73 0.42	k
19.7	Los Alamos76 8	13σ	0.37		0.9956	9.20	6.21	$^1S_0 = 51.23 \pm 0.13$ $\Delta_C = 0.482 \pm 0.025$	51.09 0.498	

TABLE III. (*Continued*).

T_{lab} (MeV)	Institute, Reference	Number, Type of data[a]	% norm error	Deleted data	Predicted norm[b]	χ^2_{me}	χ^2_{sg}	sg phases	me phases	Comments
20.2	Saclay68 84	8*P*	12.0	all						h
21.95, . . . , 30.33	Rutherford64 85	2σ	0.36	21.95 MeV	1.0012	0.29	0.12	$^1S_0 = 48.27 \pm 0.17$ at 25.62 MeV	48.51	d,n
25.63	Minnesota60 86	23σ	0.93	all						k,h
26.5	Saclay70 87	1A_{xx} 1A_{yy}	∞		1.0195	0.03	0.0	$\Delta_T = -2.44 \pm 0.16$	−2.45	n
27.05	Los Alamos67 88	1A_{yy}	0.0		1.0	0.29	0.0	$\Delta_T = -2.77 \pm 0.46$	−2.49	
27.4	Harwell63 89	1*P*	0.0		1.0	0.14	0.0	$\Delta_T = -2.3 \pm 1.2$	−2.5	n,o
27.6	Rutherford65 90	3*R* 3*A*	3.0		1.0257	10.53	6.64	$\Delta_T = -1.84 \pm 0.24$ $\Delta_{LS} = 0.65 \pm 0.26$	−2.53 0.85	
28.16	Minnesota59b 91	1σ	0.0		1.0	0.22	0.0	$^1S_0 = 46.96 \pm 0.60$	47.45	k,n
30.0	Rutherford63 92	1*P*	4.0		1.0063	4.17	0.0	$\Delta_{LS} = -0.43 \pm 0.64$	0.92	n

[a]Unless all data are deleted, the number of data does not include deleted data. Experimentally determined normalizations are also not counted.
[b]Predicted norm: ν_A^{-1} arrived at in the me fit, with which the experimental values should be multiplied before comparison with the theoretical values [Eq. (66)].
[c]Two extra angle-dependent normalizations included (Ref. 3, p. 464).
[d]Individual data points rejected as $\chi^2 > 9$. Whole group of data rejected as $\chi^2 > \beta\chi^2_{high}$ (see rejection criteria).
[e]Relatively unrestrictive to the $^1S_0$ phase shift.
[f]Rejected as a result of the analysis of van der Sanden, Emmen, and de Swart (Ref. 17) of the 0–3 MeV data.
[g]Old polarization data. *P* as determined by all data is much smaller than these groups values and errors.
[h]Group rejected as $\chi^2 < \chi^2_{low}$ (see rejection criteria).
[i]We used the BGS data (Ref. 68).
[j]$\Delta\chi^2$ between me fit and sg fit too large, arising from a deviation of Δ_C.
[k]Probable errors changed to standard errors ($\sigma \approx 1.48$ probable errors).
[l]One point of this group (then at 9.68 MeV) was published in Ref. 91.
[m]In the se analysis this group was split. The 11.4 MeV data then were taken with the free norm, the other data with a fixed norm.
[n]Belongs to a group of data with points for $T_{lab} > 30$ MeV.
[o]Data as renormalized by Jarvis and Rose (Ref. 93).

table. The single-group phases of some groups deviate too much (criterion 2) from the fit-2 values and are therefore rejected. These are the two groups of Berkeley68 differential cross sections[68] (17 data at 6.141 MeV and 16 data at 8.097 MeV). Some groups have an improbably low value of χ^2 (criterion 3) in fit 2 or in the single-group fit and are therefore rejected. These are two groups of polarizations[9,84] (in total 14 data) and two groups of differential cross sections[81,86] (in total 40 data). Except for the Erlangen79 polarizations at 6.141 MeV,[9] the low χ^2 of these groups of data has been known already from earlier analyses.

From the single-group fits one can judge the importance of groups of data in the determination of the phase shifts. Section VI C deals with the se results, and some remarks are made about specific groups of data in our final data set.

After these rejections, we have arrived at our final set of data, comprising 360 observables in 30 groups, of which five have a free norm. We believe that it contains no data contradicting each other too much and no data of which the errors can be seen to contain a too-large systematic component.

As a third step, the final me fit and all se fits can be done with this final set of data. Also the single-group fits for the remaining groups have to be redone, but the difference with the previous single-group fits is very small. The results of these fits are discussed in Sec. VI.

VI. RESULTS

A. Multienergy results

Having defined our final set of data (Sec. V B), we fit the 10 P-matrix parameters for the lower partial waves (Sec. II B) and the $pp\pi^0$ coupling constant that affects all partial waves, for various values of the P-matrix radius b. For b between 1.1 and 1.7 fm we achieve a fit in which χ^2 deviates no more than 1 from the minimum. This rather weak dependence with an optimum for a reasonable value of b is satisfying. It is clear that a totally correct potential tail would have allowed smaller values for the P-matrix matching radius. Therefore one can see here that for $r \lesssim 1$ fm nuclear forces other than OPE are present. As explained in Sec. II B larger values of b shift the pole positions of the P matrix to lower energies. Since our parametrizations allow for a limited structure, the upper limit on b can be understood. We choose to give our results for $b = 1.4$ fm, which is approximately the best value. We reached $\chi^2 = 343.2$ for 343 degrees of freedom, or $\chi^2/N_{\rm df} = 1.00$. Theoretically one expects $\chi^2/N_{\rm df} = 1$, with an error $\sqrt{2/N_{\rm df}} = 0.076$. The χ^2 distribution over the individual points agrees very well with the expected statistical distribution, as is shown in the Appendix.

The values and errors for the parameters in the multienergy fit can be found in Table IV. The errors are square roots of the diagonal elements of the 11×11 error matrix.

The not very strong result for the $pp\pi^0$ coupling constant $g^2_{pp\pi^0}/4\pi = 14.5 \pm 1.2$ is in agreement with other determinations.[95] The higher partial waves ($J \geq 3$) give almost no restriction on the pion-coupling constant. Of the lower partial waves, the $^1S_0$ gives as much information on $g^2_{pp\pi^0}$ as the other partial waves. That the $^3P_2$ P-matrix parameters are determined more precisely than the P-matrix parameters for the $^3P_0$ and $^3P_1$ stems from the fact that OPE produces only a small part of the $^3P_2$ phase shift. Some reservations have to be made with respect to the results in Table IV, since the P-matrix parameters are of course model dependent. First of all, it should be noted that the values and errors of Table IV are evaluated for a fixed b. For other values of b, the P-matrix parameters to describe the same phase shifts will be different. The changes in the results that would have occurred if we had included the important unpublished data are discussed below. Another reservation that could be made is that perhaps very different P-matrix parameters would have resulted if we had chosen a different external potential (e.g., including higher-mass mesons). To judge the model dependence due to the potential tail we added to our potential tail the Nijmegen one-boson-exchange potential (N78) (Ref. 27) for $r > 1.4$ fm, except for its OPE part. With this different potential tail an equally good fit to the data is achieved. With this better potential tail $\chi^2_{\rm min}$ is even slightly worse, it rises by 0.23. The phase shifts remain essentially unchanged (compared with the accuracy with which they are determined). Satisfying is that even the pion-coupling constant arrived at in this way ($g^2_{pp\pi^0}/4\pi = 14.2 \pm 1.3$) does not deviate much from the value found in the me fit. The resulting

TABLE IV. Values and errors (for $b = 1.4$ fm) for the parameters. For the definition of the partial wave parameters, see Sec. II B. For comparison, the corresponding values for the free P matrix are also given. All values are in appropriate powers of fm.

Partial wave	Parameter	Fitted value	Free value
	$g^2_{pp\pi^0}/4\pi$	14.5±1.2	
$^1S_0$	c_0	0.230±0.013	1
	r_0	1.58±0.86	2
	k_0^2	3.3±1.5	5.0
$^3P_0$	c_{10}	3.39±0.77	2
	d_{10}	−2.9±1.5	−0.4
$^3P_1$	c_{11}	1.70±0.48	2
	d_{11}	−0.25±0.86	−0.39
$^3P_2$-ϵ_2-$^3F_2$	c_{12}	1.355±0.030	2
	d_{12}	−0.20±0.16	−0.39
$^1D_2$	c_2	1.01±0.31	3

P-matrix parameters, especially for the $^1S_0$ and $^3P_2$, are that even the pion-coupling constant arrived at in this way ($g^2_{pp\pi^0}/4\pi = 14.2 \pm 1.3$) does not deviate much from the value found in the me fit. The resulting P-matrix parameters, especially for the $^1S_0$ and $^3P_2$, are quite different, from which one can see that they must be regarded as model-dependent quantities.

Table V presents in sufficient detail the me phase shifts and mixing parameters of the bar decomposition of the total S matrix (Sec. IV). Linear interpolation in T_{lab} of the phase shifts reproduces the me phase shifts at every energy with an error less than the neighboring se error bar, except for $\delta(^1S_0)$ at very low energies. The accuracy of linear interpolation of the $^1S_0$ phase shift from the table below 2 MeV is only about 10^{-2} deg. For $\delta(^1S_0)$ it is much better of course to interpolate the correct effective range function $F_{EM}(k^2)$ (see Sec. VI B), since the effective range function is developed to give a smooth parametrization for the very nonsmooth $^1S_0$ phase shift. But the interpolation of $F_{EM}(k^2)$ requires the use of nontrivial functions. A very accurate and simple way to reproduce our me $^1S_0$ phase shift at all energies is to interpolate linearly in T_{lab} (or k^2) the function

$$F = C_0^2(\eta')k\cot(\delta_0 - \tilde{\Delta}_0) + 2k\eta' h(\eta') , \tag{73}$$

with the $^1S_0$ phase shift δ_0 and the improved Coulomb-Foldy correction $\tilde{\Delta}_0$ (Sec. IV B) as given in Table V, and then to interpolate $\tilde{\Delta}_0$ linearly to get δ_0 at the required energy. The standard functions $C_0^2(\eta')$ and $h(\eta')$ in Eq. (73) are as given in Eq. (10). The accuracy with which our me $^1S_0$ phase shift is thus reproduced is about 10^{-4} deg below 2 MeV. That Eq. (73) supplies an accurate way to interpolate the $^1S_0$ phase shift is easily understood, since the improved Coulomb-Foldy correction $\tilde{\Delta}_0$ can be used to remove approximately vacuum polarization and improved Coulomb effects from the phase shift δ_0.

The phase shifts in the higher partial waves, not given in this table were taken to be improved Coulomb plus vacuum polarization plus OPE phase shifts, computed in Coulomb-distorted-wave Born approximation. Also the $^3F_2$ phase shift is not given in the table, since it surpasses the $\tilde{V}_C + V_{VP} + V_{OPE}$ value at 25 MeV only by 1.5×10^{-3} deg and the difference is less at lower energies. The ϵ_2 mixing parameter, which has been tabulated, is about 3% more negative than the $\tilde{C}$+VP+OPE value. Some phase shifts at the precise energies of the experimental data can be found in the data reference table in the column labeled me phases.

Next to the me phase shifts, one can also find in Table V the quantities that can be used to compare our phase shifts with those of models that do not incorporate vacuum polarization and/or improved Coulomb. These are τ_l, the vacuum polarization phase shift, ρ_l, the phase shift of the V_{C2} part of the improved Coulomb potential, and furthermore the Foldy correction Δ_0 and the improved Coulomb-Foldy correction $\tilde{\Delta}_0$ both calculated for the Nijmegen potential.[27] To compare our $^1S_0$ phase shift, that is the phase shift $(\delta^C_{\tilde{C}+VP+OPE})_0$ with respect to Coulomb functions (see Sec. IV), with phase shifts $(\delta^C_{C+N})_0$ of models that incorporate neither improved Coulomb nor vacuum polarization, but only the Coulomb potential V_{C1} [Eq. (25)] and a nuclear potential, one should use the relation

$$(\delta^C_{C+N})_0 = (\delta^C_{\tilde{C}+VP+N})_0 - \tilde{\Delta}_0 . \tag{74}$$

An example: The Nijmegen potential[27] gives at 25 MeV $(\delta^C_{C+N})_0 = 49.28°$. With $\tilde{\Delta}_0(25\text{ MeV}) = -0.036°$ from Table V one obtains for the Nijmegen potential $(\delta^C_{\tilde{C}+VP+N})_0 = 49.244°$ which is 3.3 se error bars larger than our se value, as can be seen in Fig. 2. For a model that incorporates vacuum polarization but not improved Coulomb, and of which the phase shift is given with respect to vacuum polarization functions, one can use

$$\tau_0 + (\delta^{C+VP}_{C+VP+N})_0 = (\delta^C_{\tilde{C}+VP+N})_0 - \tilde{\Delta}_0 + \Delta_0 . \tag{75}$$

For partial waves with $l > 0$ one does not need a table of Foldy corrections, since for reasonable nuclear potential models one has accurately enough $\Delta_l \approx \tau_l$ and $\tilde{\Delta}_l \approx \tau_l + \rho_l$. For $l > 0$ ρ_l has not been tabulated, since in good enough approximation $\rho_1 \approx 1.4 \times 10^{-3}$ deg and $\rho_2 \approx 9 \times 10^{-4}$ deg between 0.1 and 30 MeV. From the smallness of these phase shifts ρ_1 and ρ_2 one should not conclude that the V_{C2} part of the improved Coulomb potential is unimportant, because a lot of partial waves contribute due to the very long range of V_{C2}.

One can see in Table V that for low enough energy the $^1D_2$ phase shift almost equals τ_2, but the P-wave phase shifts already deviate from τ_1 at the lowest experimental energies. This difference is due to the threshold behavior of the nuclear phase shifts. The drastic fall off of the VP phase shift is only seen below about 0.1 MeV. One can also see the accidental crossing at $T_{lab} \approx 30$ MeV of Δ_0 and τ_0 and at $T_{lab} \approx 18$ MeV of $\tilde{\Delta}_0$ and τ_0. For most purposes it might be accurate enough to approximate above 30 MeV Δ_0 and $\tilde{\Delta}_0$ by τ_0.

The me phase shifts (labeled M) are also shown in Figs. 2, 3, 6, and 7. For the $^1S_0$ the direct plot of the phase

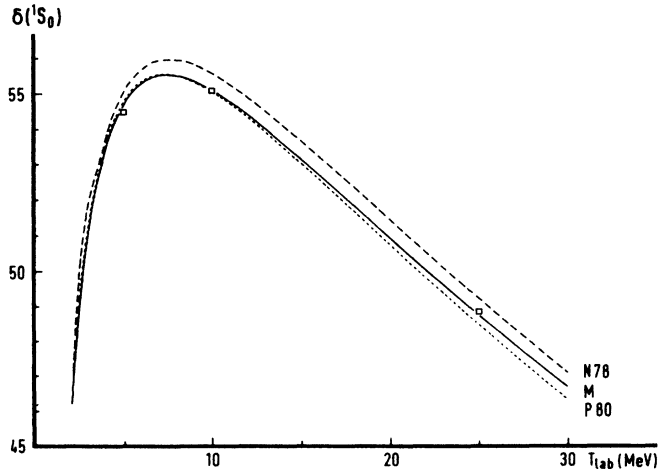

FIG. 6. $^1S_0$ phase shift δ_0 in degrees vs T_{lab}. ⊕: single-energy analyses. M: multienergy analysis. P80: Paris potential (Ref. 28). N78: Nijmegen potential (Ref. 27).

TABLE V. Multienergy phase shifts and mixing parameter with respect to Coulomb functions in degrees (from the decomposition of the total S matrix) as a function of T_{lab} (MeV). For the (improved Coulomb-) Foldy corrections Δ_0 and $\tilde{\Delta}_0$ of the Nijmegen78 potential and the improved Coulomb phase shift ρ_l, see Eqs. (42), (60), and (61). In Sec. VI A the use of the table is demonstrated.

T_{lab}	$^1S_0$	$^3P_0$	$^3P_1$	$^3P_2$	$^1D_2$	ϵ_2	Δ_0	$\tilde{\Delta}_0$	τ_0	τ_1	τ_2	ρ_0
0.10	2.2966	−0.050	−0.052	−0.051	−0.030	0.000	−0.1211	−0.1170	−0.1006	−0.053	−0.031	0.0026
0.15	4.4522	−0.051	−0.056	−0.054	−0.033	0.000	−0.1424	−0.1367	−0.1064	−0.055	−0.034	0.0029
0.20	6.6983	−0.049	−0.059	−0.054	−0.034	0.000	−0.1581	−0.1508	−0.1079	−0.056	−0.035	0.0031
0.25	8.9299	−0.045	−0.062	−0.054	−0.035	0.000	−0.1705	−0.1618	−0.1077	−0.056	−0.036	0.0033
0.30	11.1025	−0.041	−0.064	−0.054	−0.036	0.000	−0.1806	−0.1705	−0.1069	−0.056	−0.037	0.0034
0.35	13.1953	−0.036	−0.067	−0.053	−0.036	0.000	−0.1889	−0.1776	−0.1057	−0.056	−0.037	0.0035
0.40	15.1986	−0.030	−0.071	−0.052	−0.036	0.000	−0.1956	−0.1832	−0.1045	−0.056	−0.037	0.0036
0.45	17.1088	−0.023	−0.075	−0.051	−0.036	0.000	−0.2011	−0.1877	−0.1032	−0.056	−0.037	0.0037
0.50	18.9251	−0.016	−0.079	−0.050	−0.036	0.000	−0.2054	−0.1911	−0.1019	−0.055	−0.037	0.0037
0.55	20.6492	−0.009	−0.083	−0.049	−0.036	0.000	−0.2087	−0.1936	−0.1006	−0.055	−0.037	0.0038
0.60	22.2837	−0.001	−0.088	−0.048	−0.036	0.000	−0.2111	−0.1954	−0.0994	−0.055	−0.037	0.0038
0.65	23.8319	0.008	−0.092	−0.046	−0.036	0.000	−0.2128	−0.1965	−0.0982	−0.054	−0.037	0.0038
0.70	25.2976	0.016	−0.098	−0.045	−0.035	0.000	−0.2138	−0.1970	−0.0971	−0.054	−0.037	0.0039
0.75	26.6850	0.026	−0.103	−0.044	−0.035	−0.001	−0.2144	−0.1971	−0.0960	−0.054	−0.037	0.0039
0.80	27.9980	0.035	−0.109	−0.042	−0.035	−0.001	−0.2144	−0.1968	−0.0949	−0.053	−0.037	0.0039
0.85	29.2407	0.045	−0.115	−0.041	−0.035	−0.001	−0.2140	−0.1961	−0.0940	−0.053	−0.036	0.0040
0.90	30.4171	0.056	−0.121	−0.039	−0.035	−0.001	−0.2133	−0.1951	−0.0930	−0.052	−0.036	0.0040
0.95	31.5311	0.066	−0.127	−0.038	−0.034	−0.001	−0.2123	−0.1939	−0.0921	−0.052	−0.036	0.0040
1.00	32.5864	0.077	−0.134	−0.036	−0.034	−0.001	−0.2111	−0.1925	−0.0912	−0.052	−0.036	0.0040
1.10	34.5347	0.100	−0.147	−0.033	−0.034	−0.002	−0.2081	−0.1893	−0.0896	−0.051	−0.036	0.0041
1.20	36.2878	0.124	−0.162	−0.030	−0.033	−0.002	−0.2045	−0.1857	−0.0880	−0.051	−0.036	0.0041
1.30	37.8689	0.149	−0.177	−0.026	−0.032	−0.002	−0.2007	−0.1818	−0.0866	−0.050	−0.035	0.0041
1.40	39.2980	0.175	−0.192	−0.023	−0.032	−0.003	−0.1966	−0.1778	−0.0853	−0.049	−0.035	0.0041
1.50	40.5927	0.202	−0.209	−0.019	−0.031	−0.003	−0.1924	−0.1737	−0.0840	−0.049	−0.035	0.0042
1.60	41.7684	0.230	−0.225	−0.015	−0.030	−0.004	−0.1882	−0.1697	−0.0829	−0.048	−0.035	0.0042
1.70	42.8385	0.258	−0.243	−0.011	−0.029	−0.005	−0.1841	−0.1657	−0.0818	−0.048	−0.034	0.0042
1.80	43.8145	0.288	−0.260	−0.007	−0.029	−0.005	−0.1800	−0.1619	−0.0807	−0.047	−0.034	0.0042
1.90	44.7067	0.318	−0.278	−0.003	−0.028	−0.006	−0.1761	−0.1581	−0.0798	−0.047	−0.034	0.0042

TABLE V. (*Continued*).

T_{lab}	$^1S_0$	$^3P_0$	$^3P_1$	$^3P_2$	$^1D_2$	ϵ_2	Δ_0	$\tilde{\Delta}_0$	τ_0	τ_1	τ_2	ρ_0
2.00	45.5237	0.348	−0.297	0.002	−0.027	−0.007	−0.1722	−0.1545	−0.0788	−0.047	−0.034	0.0042
2.10	46.2734	0.379	−0.316	0.006	−0.026	−0.008	−0.1685	−0.1510	−0.0779	−0.046	−0.033	0.0043
2.20	46.9625	0.411	−0.335	0.011	−0.025	−0.009	−0.1649	−0.1476	−0.0771	−0.046	−0.033	0.0043
2.30	47.5970	0.444	−0.354	0.016	−0.024	−0.010	−0.1614	−0.1444	−0.0763	−0.045	−0.033	0.0043
2.40	48.1820	0.476	−0.374	0.021	−0.023	−0.011	−0.1581	−0.1413	−0.0755	−0.045	−0.033	0.0043
2.50	48.7224	0.510	−0.394	0.026	−0.022	−0.012	−0.1549	−0.1384	−0.0748	−0.045	−0.033	0.0043
2.60	49.2220	0.543	−0.415	0.031	−0.020	−0.013	−0.1518	−0.1355	−0.0741	−0.044	−0.032	0.0043
2.70	49.6846	0.578	−0.435	0.036	−0.019	−0.014	−0.1489	−0.1328	−0.0734	−0.044	−0.032	0.0043
2.80	50.1135	0.612	−0.456	0.041	−0.018	−0.016	−0.1461	−0.1302	−0.0728	−0.044	−0.032	0.0043
2.90	50.5114	0.647	−0.477	0.047	−0.017	−0.017	−0.1433	−0.1277	−0.0722	−0.044	−0.032	0.0043
3.00	50.8810	0.683	−0.498	0.052	−0.015	−0.018	−0.1407	−0.1253	−0.0716	−0.043	−0.032	0.0043
4.00	53.4324	1.052	−0.718	0.113	0.000	−0.035	−0.1196	−0.1060	−0.0665	−0.041	−0.030	0.0044
5.00	54.7069	1.441	−0.945	0.183	0.019	−0.056	−0.1048	−0.0927	−0.0628	−0.039	−0.029	0.0045
6.00	55.3145	1.840	−1.175	0.261	0.041	−0.082	−0.0940	−0.0829	−0.0598	−0.037	−0.028	0.0045
7.00	55.5401	2.241	−1.403	0.346	0.066	−0.111	−0.0857	−0.0755	−0.0573	−0.036	−0.027	0.0045
8.00	55.5323	2.642	−1.628	0.438	0.093	−0.143	−0.0791	−0.0696	−0.0553	−0.035	−0.027	0.0045
9.00	55.3755	3.039	−1.848	0.536	0.123	−0.178	−0.0737	−0.0648	−0.0535	−0.034	−0.026	0.0446
10.00	55.1205	3.430	−2.063	0.639	0.155	−0.215	−0.0692	−0.0608	−0.0519	−0.033	−0.026	0.0046
12.00	54.4331	4.193	−2.474	0.858	0.223	−0.294	−0.0622	−0.0546	−0.0493	−0.032	−0.025	0.0046
14.00	53.6183	4.928	−2.860	1.092	0.297	−0.379	−0.0569	−0.0499	−0.0472	−0.031	−0.024	0.0046
16.00	52.7461	5.636	−3.221	1.338	0.375	−0.466	−0.0527	−0.0462	−0.0454	−0.030	−0.023	0.0047
18.00	51.8526	6.321	−3.558	1.593	0.457	−0.556	−0.0494	−0.0432	−0.0439	−0.030	−0.023	0.0047
20.00	50.9572	6.987	−3.873	1.855	0.543	−0.646	−0.0466	−0.0407	−0.0426	−0.029	−0.023	0.0047
22.00	50.0710	7.641	−4.168	2.122	0.632	−0.737	−0.0442	−0.0386	−0.0414	−0.029	−0.022	0.0047
24.00	49.2001	8.287	−4.443	2.392	0.723	−0.828	−0.0421	−0.0368	−0.0404	−0.028	−0.022	0.0047
26.00	48.3481	8.933	−4.700	2.665	0.818	−0.917	−0.0403	−0.0353	−0.0394	−0.028	−0.022	0.0047
28.00	47.5168	9.584	−4.940	2.937	0.915	−1.005	−0.0388	−0.0339	−0.0386	−0.028	−0.021	0.0047
30.00	46.7072	10.246	−5.166	3.209	1.015	−1.092	−0.0374	−0.0327	−0.0378	−0.028	−0.021	0.0048

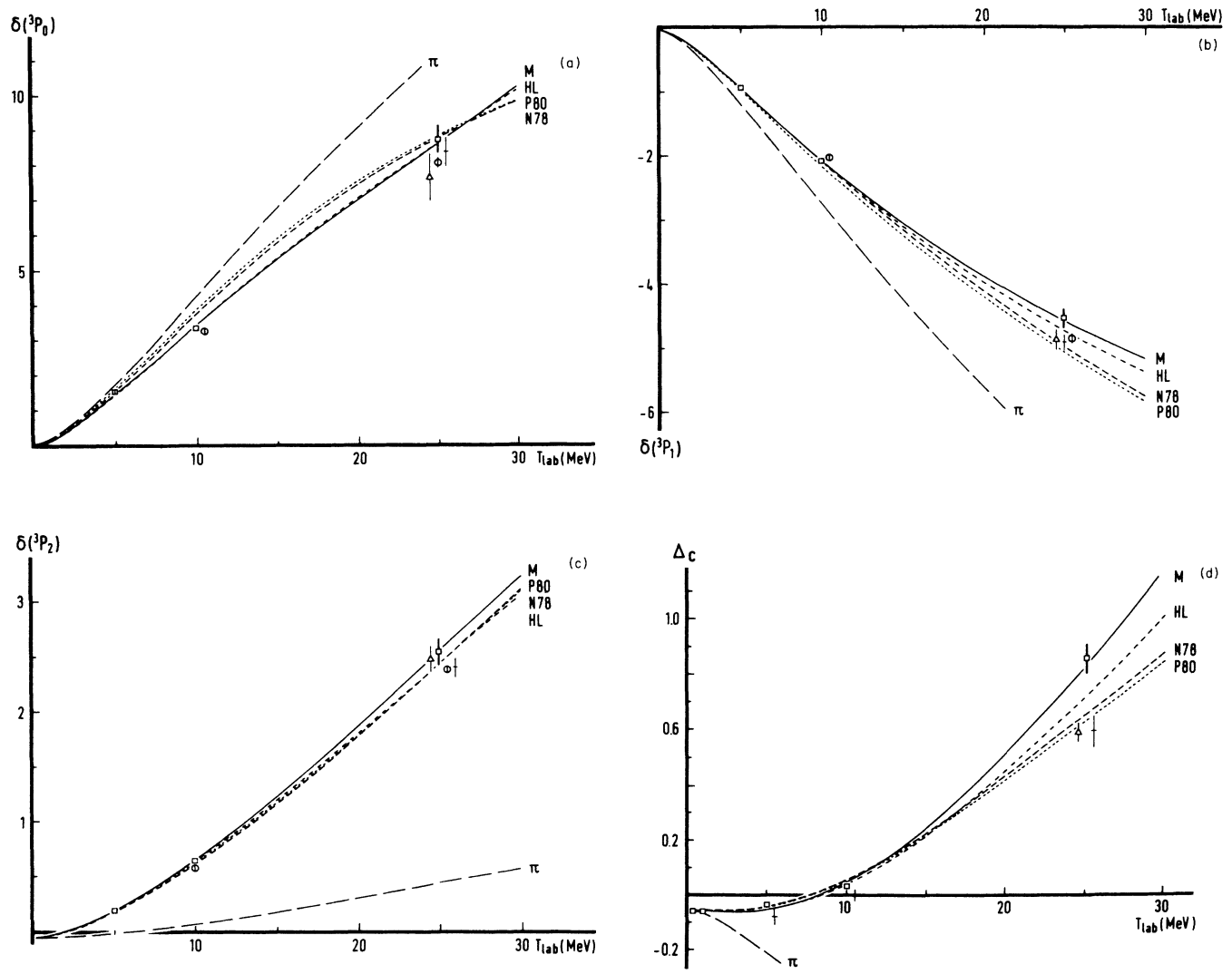

FIG. 7. *P*- and *D*-wave phase shifts δ in degrees vs $T_{\rm lab}$. ⊕: single-energy analyses. *M*: multienergy analysis. HL: me fit with unpublished data (Refs. 29–32) included. ϕ: Arndt *et al.* (Ref. 36). ⊦: SSH (Ref. 12). ⍋: Bohannon, Burt, and Signell (Ref. 40). N78: Nijmegen78 potential (Ref. 27). P80: Paris80 potential (Ref. 28). π: One-pion exchange.

shift (Fig. 6) can hardly show the fantastic accuracy with which the $^1S_0$ is determined. Therefore in Figs. 2 and 3 the shape $S_{\rm EM}(T_{\rm lab})$ is displayed. The shape is the deviation of the effective range function $F_{\rm EM}$ (Sec. VI B) from the straight line

$$S_{\rm EM}=F_{\rm EM}-\left[-\frac{1}{a_{\rm EM}}+\frac{1}{2}r_{\rm EM}k^2\right],$$

where the effective range parameters $a_{\rm EM}$ and $r_{\rm EM}$ are determined from the $^1S_0$ phase shift of the me fit.

The effect of our rejection of the unpublished Minnesota77 (Refs. 29 and 30) and Los Alamos76 (Refs. 31 and 32) data can be seen in the lines labeled HL. These would be the result of the me fit if we included these important unpublished data.[29–32] Since the group of Minnesota77 differential cross sections at 13.6 MeV would not have survived our rejection criteria, these data have not been included here. Whether deviations are of significance can be seen by comparing them with our se error bars (⊕). The most important of the differences between the *M* and HL lines, due to the Minnesota77 (Refs. 29 and 30) data, are found for $\delta(^1S_0)$, Δ_C, and $\delta(^1D_2)$ for energies $T_{\rm lab}>10$ MeV. Including the Minnesota77 data furthermore would result in a pion-coupling constant $g^2_{{\rm pp}\pi^0}/4\pi$ that is about one standard deviation smaller (13.4 ± 1.0). Preliminary analysis indicates that inclusion of data around $T_{\rm lab}=50$ MeV shows the same trends as inclusion of the Minnesota77 (Refs. 29 and 30) data.

The above-mentioned differences between the phase shifts of these modified analyses and our me analysis are 1–2 standard deviations (s.d.). Since these modified analyses show the same trends, we are led to the belief that, e.g., the pion-coupling constant is more likely to be small-

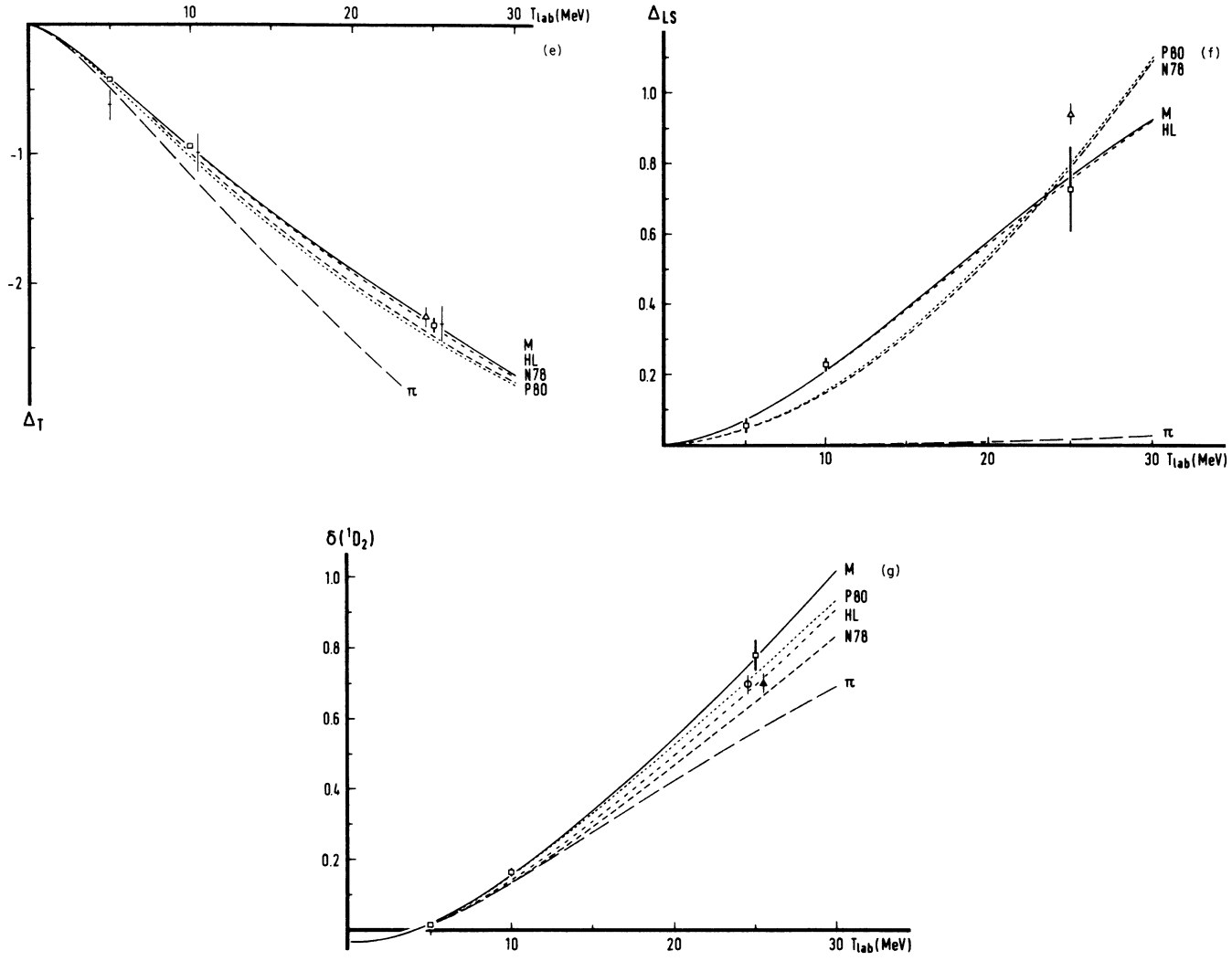

FIG. 7. (*Continued*).

er than 14.5, the value found in the me fit. For $\delta(^1S_0)$, Δ_C, and $\delta(^1D_2)$, we have analogous beliefs. Probably these problems arise because of the rather small number of data available at the end of our energy range. Further analysis up to higher energies will have to show whether these beliefs are well founded. The situation could also be clarified by new differential cross-section experiments above about 15 MeV. Other types of experiments could also greatly improve the data set above about 15 MeV. For the pion-coupling constant the results from a 0–350 MeV analysis have already been reported,[96] giving indeed a lower value ($g^2_{pp\pi^0}/4\pi = 13.1 \pm 0.1$) than this analysis.

Phase shifts calculated with the OPE (π), the Nijmegen (N78) (Ref. 27) and the Paris (P80) (Ref. 28) potential are also shown in the figures. To these nuclear potentials we added the electromagnetic potential: improved Coulomb and vacuum polarization. We do not compare with other nucleon-nucleon potential results, since unfortunately enough we do not have a computer code to calculate the Funabashi potentials,[97–99] and the Bonn[100–102] and Argonne[103] potentials are neutron-proton potentials. As for the $^1S_0$ in Figs. 2 and 3 one can see that for very low energies the Paris (P80) (Ref. 28) potential is very much in error, since its $\delta(^1S_0)$ is 0.14° (57 s.d.) too large at the interference minimum and 0.24° (26 s.d.) too large at 1 MeV, but above about 3 MeV it is somewhat better than the Nijmegen (N78) (Ref. 27) potential. If one would add only the standard Coulomb and the vacuum polarization potential to the Paris potential and not the improved Coulomb potential, the difference with our analysis would be slightly less (0.01–0.02°) at these energies. That the Paris potential[28] gives wrong values for the $^1S_0$ scattering length a^C and effective range r^C was already noted by Piepke.[104] We obtain the same values. We have included in the Paris potential the proper electromagnetic potential. Contrary to the explanation accepted by Piepke,[104] inclusion of vacuum polarization in the Paris potential for the $^1S_0$ can accurately be approximated by the Foldy correction Δ_0. Perhaps the easiest way to ensure a reasonable low-energy behavior of potential models is to fit the $^1S_0$ phase shift at the interference minimum at 1 MeV. This is easier than fitting effective range parameters. The comparison of the $^1S_0$ results with those of earlier low-energy analyses is made

in terms of effective range parameters in Sec. VI B. No comparison is made there with the series of analyses of Arndt *et al.*,[34–37] since these are not intended to be detailed low-energy analyses but aim primarily at the higher energies. This can be seen in several ways. First of all, below 25 MeV, Arndt *et al.*[36] do not give a se $\delta(^1S_0)$; at 25 MeV their se $\delta(^1S_0)$ is in accordance with ours (Sec. VI B) but their me $\delta(^1S_0)$ is 0.7° (3.2 s.d.) lower than their own se $\delta(^1S_0)$ and 0.9° (8 s.d.) lower than our se $\delta(^1S_0)$. Thus probably their parametrization of the phase shifts as a function of the energy is not good enough. At 10 MeV the difference between their me $\delta(^1S_0)$ and ours is about the same as at 25 MeV. Furthermore, Arndt *et al.*[36] do not give error bars for the combinations of *P*-wave phase shifts Δ_C, Δ_T, and Δ_{LS}. In their latest analysis[37] dramatic changes in the 10, 25, and 50 MeV np se phase shifts (up to 9 s.d.) are left undiscussed.

For the ^3P waves in Figs. 7(a)–7(c) one can see that the Nijmegen (N78) and Paris (P80) (Refs. 27 and 28, respectively) potentials predict a too-large $\delta(^3P_0)$ around 10 MeV. It is more instructive to look at the combinations of ^3P-wave phase shifts Δ_C, Δ_T, and Δ_{LS} in Figs. 7(d)–7(f), since in Born approximation the central, tensor, and spin-orbit parts of the potentials are responsible for these combinations. One can see that the central *P*-wave combination Δ_C of this analysis above 20 MeV is substantially larger than those of the older analyses of SSH[12] and Bohannon, Burt, and Signell.[40] As mentioned above, inclusion of unpublished data and a preliminary analysis of higher energy data up to about 50 MeV both give also a somewhat smaller Δ_C. Whether or not our high Δ_C around 25 MeV should be viewed as a statistical fluctuation that has a large effect since it occurs at the end of our energy range will become clearer when we finish the analysis up to higher energies. For Δ_T and Δ_{LS} the most important features are (i) Our se error bars at 5 and 10 MeV are much smaller than those of previous analyses, due to the new Wisconsin82 (Refs. 6 and 7) analyzing power data. In the same publication[6,7] Barker *et al.* reported also an analysis, which, however, was in error, giving a Δ_T deviating more than 3 s.d. from what we find for their data. (ii) Both the Nijmegen (N78) (Ref. 27) and the Paris (P80) (Ref. 28) potential give a too large Δ_T and a too small Δ_{LS} at 10 MeV. This has already been discussed elsewhere.[105] Probably this shows a flaw in the treatment of the medium range forces in these potential models. As one can see in Fig. 7(f) OPE gives only a very small Δ_{LS} [in Born approximation $\Delta_{LS}(\text{OPE})=0$], and therefore in Δ_{LS} interactions of shorter range (e.g., two-pion exchange or ϵ exchange) are visible.

B. Effective range parameters

In the low-energy domain, results of an analysis are often presented in terms of effective range (ER) parameters.[15,12,16,2,17] In order to make a comparison with those analyses, we give the values that can be deduced from the behavior near $k^2=0$ of our multienergy phase shifts. The error on the ER parameters is the maximum deviation possible without raising χ^2 by more than 1 in varying the 10 *P*-matrix parameters and the pion-coupling constant. For the $^1S_0$ phase shift we used the ER function for $\delta_0^{\rm EM}$ as given by van der Sanden, Emmen, and de Swart[17]

$$F_{\rm EM}(k^2)=C_0^2(\eta')k\frac{(1+\chi_0)\cot\delta_0^{\rm EM}-\tan\tau_0}{(1+A_1)(1-\chi_0)}$$
$$+(1-A_2)2\eta' k h(\eta')$$
$$+k^2 d[C_0^4(\eta')-1]+2\eta' k l_0$$
$$=\frac{-1}{a_{\rm EM}}+\frac{1}{2}r_{\rm EM}k^2+\mathcal{O}(k^4)\ . \qquad (76)$$

The definitions of χ_0 and l_0 can be found in Ref. 19, those of d, A_1, and A_2 in Ref. 17. If one ignores the relativistic correction V_{C2} to the static Coulomb potential $V_{C1}=\alpha'/r$, i.e., taking d, A_1, and A_2 equal to zero, one gets back the ER function of Heller.[19] Ignoring this correction in an analysis results in a value for $a_{\rm EM}$ that is about 0.009 fm more negative and about the same value for $r_{\rm EM}$.[17] Since Naisse[2] uses the ER function for δ^C, the Coulomb corrections in the $^1S_0$ partial wave are treated in a model-dependent manner in that analysis. We have used the improved Coulomb-Foldy correction $\tilde{\Delta}_0$ (Secs. IV B and VI A) to compute the values of our multienergy δ^C in order to compare with his results (a^C and r^C). It should be emphasized here again that $\tilde{\Delta}_0$ corrects only for vacuum polarization and improved Coulomb (see also Sec. IV B), where the protons are treated as point charges. Ideally one would have an electromagnetic Foldy correction that corrects for all electromagnetic effects, except for the point Coulomb interaction V_{C1}. The most important electromagnetic effect not included in our improved Coulomb-Foldy correction is the change in the Coulomb potential due to the spatial extension of the charges. It is not necessary to incorporate that in our potential tail, since it is of short range and can therefore be absorbed in the *P* matrix. But it will be the major error made if one adjusts the parameters of a nuclear potential plus V_{C1} to fit our values of a^C and r^C. The elimination of this error is under study[67] with the Nijmegen potential[27] as the nuclear potential. Preliminary results are that elimination of this error makes a^C about 0.0075 fm more negative and r^C about 0.002 fm less positive.

The region of convergence of the ER series of Eq. (76) is determined by the logarithmic singularity of OPE: $T_{\rm lab}<9.81$ MeV. It has been shown[17,14] that the CFS approximation as used by Noyes,[11] Naisse,[2] and Matheltsch and VerWest[18] is not accurate enough (see Sec. II). Values and errors for the $^1S_0$ ER parameters are given in Table VI, where they can be compared with earlier analyses. One can see that the (new) Zürich78 data[3] make the determination of the ER parameters more precise, and that there is a very good agreement with the analyses of Noyes[11] and Gursky and Heller.[15]

The difference between our results for the $^1S_0$ ER parameters and those of van der Sanden, Emmen, and de Swart[17] are primarily due to the difference in higher ener-

TABLE VI. $^1S_0$ scattering length and effective range (as defined in Sec. VI B) of this and earlier analyses. For van der Sanden, Emmen, and de Swart (Ref. 17) we give their values determined by the Zürich78 (Ref. 3) data. Values between parentheses give information identical to that of the line above.

Analysis	Scattering length (fm)	Effective range (fm)
Present work	$a_{\rm EM}=-7.8063\pm0.0026$	$r_{\rm EM}=2.794\pm0.014$
	$(a_E=-7.8153\pm0.0026)$	$(r_E=2.794\pm0.014)$
	$(a^C=-7.8196\pm0.0026)$	$(r^C=2.790\pm0.014)$
van der Sanden, Emmen, and de Swart[a]	$a_{\rm EM}=-7.8016\pm0.0029$	$r_{\rm EM}=2.773\pm0.014$
	$(a_E=-7.8106\pm0.0029)$	$(r_E=2.773\pm0.014)$
Gursky and Heller[b]	$a_E=-7.815\pm0.008$	$r_E=2.795\pm0.025$
Noyes and Lipinski[c]	$a_E=-7.8146\pm0.0054$	$r_E=2.795\pm0.008$
SSH[d]	$a_E=-7.821\pm0.004$	$r_E=2.830\pm0.017$
Naisse[e]	$a^C=-7.828\pm0.008$	$r^C=2.80\pm0.02$

[a]Reference 17.
[b]Reference 15.
[c]Reference 11.
[d]Reference 12.
[e]Reference 2.

gy data. They use the 0–3 MeV data and the restriction $\delta(^1S_0)=0$ at $T_{\rm lab}=253$ MeV, whereas we use the data up to 30 MeV. Inclusion of the unpublished Minnesota77 (Refs. 29 and 30) differential cross sections would have shifted our results for the $^1S_0$ ER parameters somewhat (0.6 s.d.) towards those of van der Sanden, Emmen, and de Swart.[17] The low-energy data determine $\delta(^1S_0)$ very precisely at the interference minimum ($T_{\rm lab}\approx0.38254$ MeV) and at 1 MeV. Due to the me parametrization, the ER parameters (determined at $T_{\rm lab}=0$) are sensitive to the higher-energy data. Due to this uncertainty it is probably best to recommend values for the $^1S_0$ ER parameters that are in good accordance with the 0–3 MeV as well as with the 0–30 MeV analysis: $a_{\rm EM}=-7.804\pm0.004$ fm and $r_{\rm EM}=2.784\pm0.020$ fm.

For the ^3P waves we used ER functions for δ^C_{1J} analogous to those of Heller.[19] (For $l\neq0$, $\delta^{\rm EM}_{lJ}\approx\delta^C_{lJ}$, see Sec. IV.) These ER functions $(F_C)_{1J}$ and their corresponding expansions are

$$\begin{aligned}(F_C)_{1J}&=(1+\eta'^2)k^2[C_0^2(\eta')k\cot(\delta^C_{1J})+2\eta' kh(\eta')]\\&=\frac{-1}{a_{1J}}+\frac{1}{2}r_{1J}k^2+\mathcal{O}(k^4)\quad\text{for } J=0,1\ ,\\(F_C)_{12}&=(1+\eta'^2)k^2\{C_0^2(\eta')k\cot[\delta^C_{12}-\delta^C_{12}(\text{OPE})]\\&\qquad+2\eta' kh(\eta')\}\\&=\frac{-1}{a_{12}}+\frac{1}{2}r_{12}k^2+\mathcal{O}(k^4)\ ,\end{aligned}\tag{77}$$

where in the $^3P_2$ ER function the Coulomb plus OPE $^3P_2$ phase shift is subtracted. The latter phase shift of course depends on the pion-coupling constant. The results for the deduced ^3P-wave ER parameters can be found in Table VII, where they can be compared with earlier analyses. Especially the (new) Wisconsin82 (Refs. 6 and 7) polarization data make the determination of the parameters more precise. Our values agree with those of SSH,[12] except for the $^3P_0$ with Naisse's SSH/SC values,[2] and except for the $^3P_2$ effective range with the van der Sanden 1982 analysis (in Ref. 95). All our values except for the $^3P_2$ scattering length are in disagreement with the analysis of Mathelitsch and VerWest.[18] We see no valid reason why Mathelitsch and VerWest[18] could get such small errors for their ER parameters.

If we had included the unpublished Minnesota77 differential cross sections[29,30] and the Los Alamos76 polarizations,[31,32] the $^3P_1$ scattering length would have been lowered by 0.052 fm^3 (1.2 s.d.) and the $^3P_0$ scattering length would have become 0.09 fm^3 (1 s.d.) less negative. All other ER parameters would have changed by 0.4–0.7 s.d.

C. Single-energy results

If one wants to adjust the parameters of a model to the data, one needs single-energy phases and error matrices (see Sec. V). We denote the deviation of the model phase shifts from the se phases by $\mathbf{d}$, the error matrix by E, and the minimum χ^2 arrived at in the se analysis by $\chi^2_{\rm se}$. Then if the model phase shifts are not too far away from the analysis phase shifts, one can compute the model χ^2 approximately as

$$\chi^2=\chi^2_{\rm se}+\mathbf{d}^T E^{-1}\mathbf{d}\ .\tag{78}$$

It should be noted that this representation of the χ^2 hypersurface is not an exact representation for several reasons. First of all, higher l phase shifts (pion-coupling constant) have been fixed. Furthermore, the data have been clustered at the central energies with help of the multienergy-fit results, and next to that the χ^2 hypersurface is only quadratic in the neighborhood of the

TABLE VII. Effective range parameters of the ^3P waves (in appropriate powers of fm) of this and earlier analyses. SSH (Ref. 12) give ^3P-wave parameters for three different data sets. We give here their results excluding all Wisconsin66 and Berkeley68 (Refs. 69 and 68, respectively) data, since we reject these data. Naisse (Ref. 2) discusses different models that give rather different results. We quote here his SSH/SC results.

Present work	$a_{10}=-3.03\pm0.11$	$a_{11}=2.013\pm0.053$	$a_{12}=-0.306\pm0.015$
	$r_{10}=4.22\pm0.11$	$r_{11}=-7.92\pm0.17$	$r_{12}=4.2\pm1.6$
van der Sanden	$a_{10}=-2.71\pm0.34$	$a_{11}=1.97\pm0.09$	$a_{12}=-0.316\pm0.016$
Emmen, and de Swart[a]	$r_{10}=3.8\pm1.1$	$r_{11}=-8.27\pm0.37$	$r_{12}=7.8\pm2.0$
SSH[b]	$a_{10}=-2.6\pm2.0$	$a_{11}=2.8\pm1.3$	$a_{12}=-0.45\pm0.28$
	$r_{10}=4.3\pm2.0$	$r_{11}=-9.0\pm1.0$	$r_{12}=15\pm10$
Naisse[c]	$a_{10}=-4.3\pm0.6$	$a_{11}=2.2\pm0.5$	$a_{12}=-0.30\pm0.01$
	$r_{10}=5.32\pm0.10$	$r_{11}=-8.0\pm0.2$	$r_{12}=5.5\pm0.9$
Mathelitsch	$a_{10}=-2.84\pm0.02$	$a_{11}=1.90\pm0.01$	$a_{12}=-0.31\pm0.01$
and VerWest[d]	$r_{10}=4.45\pm0.05$	$r_{11}=-7.56\pm0.05$	$r_{12}=7.59\pm0.28$

[a]Reference 95.
[b]Reference 12.
[c]Reference 2.
[d]Reference 18.

minimum. Still, this representation is much better than giving only phase shifts and errors.

To make such a representation of the χ^2 hypersurface, we divided the data into clusters around 0.382 54 MeV (the interference minimum), 1, 5, 10, and 25 MeV. We had to split one group,[80] because it contained data from 11 to 26 MeV. From these clusters we determined the single-energy phases and inverse error matrices of Table VIII in the same way as we determined single-group phases for groups with data points at different energies (Sec. V B). So for each phase shift searched for, we fitted a constant to be added to the energy-dependent P matrix of the multienergy fit. As this appeared to work not too well for the ϵ_2, we fitted here a constant to be added to the multienergy ϵ_2 mixing parameter.

Around the interference minimum and at 1 MeV only cross-section data are available. The more important groups are 5 (of the 7) new Zürich78 (Ref. 3) groups of Thomann *et al.* and the Los Alamos64 (Ref. 70) data of Brolley *et al.* These data pin down the $^1S_0$ phase shift very precisely, as is explained very nicely in the excellent 1964 analysis of the Los Alamos data by Gursky and Heller.[15] From these cross sections only the $^1S_0$ phase shift and the ^3P phase shift combination Δ_C [Eq. (19)] can be determined. We varied Δ_C by varying all ^3P_J P matrices, with fixed Δ_T and Δ_{LS}.

Around 5 and 10 MeV the new Wisconsin82 (Refs. 6 and 7) polarization data of Barker *et al.* allow a very precise determination of Δ_T and Δ_{LS}. The only cross-section data in the 5 MeV cluster are two (out of three) Kyoto75 groups of Imai *et al.*[75] Around 10 MeV one has more cross-section data and from different experimental groups. Both Kyoto75 groups[75] prefer a $^1S_0$ phase shift that is 2 s.d. smaller than our me $\delta(^1S_0)$. This is the reason for the difference between the se and me $\delta(^1S_0)$. As one can see in the data reference table, there is also friction in Δ_C between all three Kyoto75 groups[75] and the other differential cross-section data around 10 MeV.[77–79] The Kyoto75 (Ref. 75) data prefer Δ_C to be 0.02–0.03° larger than the me fit, which is 1.5–2 single-group standard deviations. The other cross-section data prefer Δ_C to be 0.05–0.09° smaller than the me fit, which is 1–2.7 single-group standard deviations.

At 5 MeV as well as at 10 MeV the clusters determine $\delta(^1S_0)$, $\delta(^3P_0)$, $\delta(^3P_1)$, $\delta(^3P_2)$, and $\delta(^1D_2)$. But the optimum values for these phase shifts depend slightly on the ϵ_2 mixing parameter. The value of ϵ_2 cannot be determined from these data, as the χ^2 reached in the se fits is virtually the same for ϵ_2 deviating up to 20% from the Coulomb plus OPE value. Therefore we give at 5 and 10 MeV the inverse error matrix

$$\left[E_{ij}^{-1}=\frac{1}{2}\frac{d^2\chi^2}{d\delta_i d\delta_j}\right]$$

as an almost degenerate 6×6 matrix. As errors for the phase shifts we give the values for ϵ_2 fixed at the me value, i.e., the values computed from the 5×5 submatrix.

At 25 MeV the cluster is rather small, though it consists of data between 18 and 30 MeV. The only new (post 1975) group in this cluster is the Los Alamos76 (Ref. 8) 19.7 MeV group of cross sections. More partial waves are important at this energy. The observables in this cluster are quite insensitive to F waves deviating up to 10% from Coulomb plus OPE. We do find a minimum in χ^2 with respect to variations in $\delta(^1S_0)$, $\delta(^3P_0)$, $\delta(^3P_1)$, $\delta(^3P_2)$, $\delta(^1D_2)$, and the ϵ_2 mixing parameter, but the value of ϵ_2 then reached is 0.27° lower than the me fit, which is 3 se standard deviations. As the ϵ_2 value of Arndt *et al.*[36,37] does not deviate much from OPE, we do not (at least until we have analyzed higher energy data) believe the 25 MeV cluster in its determination of ϵ_2. [In Sec. VI A we already discussed the $\delta(^1S_0)$ and Δ_C values of the 25 MeV cluster.] Therefore, we give in Table VIII the values of S-, P-, and D-wave phase shifts for ϵ_2 fixed at the me value. Of course we also give the 6×6 inverse

TABLE VIII. Single-energy results at $T_{lab}=0.382\,54$, 1, 5, 10, and 25 MeV. Groups: number of groups of data in this cluster. N_{obs}: number of scattering observables in this cluster. N_{df}: number of degrees of freedom, which is N_{obs} minus the number of fitted phase shifts minus the number of groups of relative measurements (see Sec. V). The phase shifts are from the bar decomposition of the total S matrix [Eq. (43)], in degrees. The lower triangular part of the inverse error matrix (deg.$^{-2}$) is given, which is $\frac{1}{2}$ times the second derivative matrix. For comparison with our me results, the corresponding me phase shifts are also given. To enable the conversion to other types of phase shifts (Sec. IV B), we also give $\tau_l+\rho_l$ [see Eq. (53)]. For $l=0$ also $\tilde{\Delta}_0$ is given, the improved Coulomb-Foldy correction [see Eq. (61)] of the Nijmegen potential (Ref. 27).

0.38254 MeV

Groups	N_{obs}	N_{df}	χ^2_{se}		
6	122	118	132.77		
Phase	me	se	Error (se)	$\tau_l+\rho_l$	$\tilde{\Delta}_0$
$^1S_0$	14.5096	14.5094	0.0025	−0.1013	−0.1814
Δ_C	−0.0559	−0.0601	0.0018	−0.0547	
Inverse error matrix (E^{-1})					
0.1683×10^6					
0.4750×10^5	0.3164×10^6				

1.0 MeV

Groups	N_{obs}	N_{df}	χ^2_{se}		
2	57	55	38.75		
Phase	me	se	Error (se)	$\tau_l+\rho_l$	$\tilde{\Delta}_0$
$^1S_0$	32.5864	32.6006	0.0094	−0.0872	−0.1925
Δ_C	−0.0561	−0.0599	0.0035	−0.0503	
Inverse error matrix (E^{-1})					
0.1214×10^5					
0.7999×10^4	0.8799×10^5				

5.0 MeV

Groups	N_{obs}	N_{df}	χ^2_{se}		
3	45	40	31.45		
Phase	me	se	Error (se)	$\tau_l+\rho_l$	$\tilde{\Delta}_0$
$^1S_0$	54.707	54.515	0.087	−0.058	−0.093
$^3P_0$	1.441	1.527	0.091	−0.037	
$^3P_1$	−0.945	−0.932	0.027	−0.037	
$^3P_2$	0.183	0.183	0.015	−0.037	
$^1D_2$	0.0186	0.0118	0.0097	−0.0282	
ϵ_2	−0.0562	−0.0562			
Inverse error matrix (E^{-1})					
0.1521×10^3					
0.3289×10^2	0.3537×10^3				
0.5127×10^2	0.8088×10^3	0.3266×10^4			
0.8064×10^2	0.7872×10^3	0.1333×10^4	0.7128×10^4		
0.3454×10^3	-0.1269×10^4	-0.3424×10^4	-0.6101×10^4	0.1918×10^5	
0.7319×10^1	-0.1021×10^3	0.3528×10^0	-0.1034×10^4	0.1472×10^4	0.2159×10^3
Phase	me	se	Error (se)	$\tau_l+\rho_l$	
Δ_C	−0.053	−0.039	0.010	−0.037	
Δ_T	−0.410	−0.419	0.017	0	
Δ_{LS}	0.072	0.055	0.015	0	

TABLE VIII. (*Continued*).

10.0 MeV

Groups	N_{obs}	N_{df}	χ^2_{se}		
9	95	88	82.37		
Phase	me	se	Error (se)	$\tau_l+\rho_l$	$\tilde{\Delta}_0$
$^1S_0$	55.121	55.108	0.068	−0.047	−0.061
$^3P_0$	3.430	3.353	0.073	−0.032	
$^3P_1$	−2.063	−2.078	0.026	−0.032	
$^3P_2$	0.639	0.636	0.019	−0.032	
$^1D_2$	0.155	0.162	0.011	−0.025	
ϵ_2	−0.215	−0.215			

Inverse error matrix (E^{-1})

0.2212×10^3					
-0.4250×10^1	0.2505×10^3				
-0.2964×10^2	-0.1407×10^3	0.1902×10^4			
-0.3282×10^2	0.9332×10^2	0.7443×10^3	0.3549×10^4		
0.1936×10^3	-0.6144×10^3	-0.1656×10^4	-0.3194×10^4	0.1294×10^5	
0.5738×10^2	-0.3889×10^3	-0.3278×10^2	-0.6286×10^3	0.2668×10^4	0.9236×10^3
Phase	me	se	Error (se)	$\tau_l+\rho_l$	
Δ_C	0.048	0.033	0.017	−0.032	
Δ_T	−0.9505	−0.9427	0.0099	0	
Δ_{LS}	0.210	0.226	0.018	0	

25.0 MeV

Groups	N_{obs}	N_{df}	χ^2_{se}		
10	41	34	22.95		
Phase	me	se	Error (se)	$\tau_l+\rho_l$	$\tilde{\Delta}_0$
$^1S_0$	48.77	49.02	0.13	−0.04	−0.04
$^3P_0$	8.61	8.20	0.37	−0.03	
$^3P_1$	−4.57	−4.33	0.15	−0.03	
$^3P_2$	2.53	2.37	0.12	−0.03	
$^1D_2$	0.771	0.904	0.057	−0.021	
ϵ_2	−0.873	−1.147	0.091	0	

Inverse error matrix (E^{-1})

0.1224×10^3					
0.1339×10^2	0.2571×10^2				
-0.7481×10^2	0.1332×10^1	0.1460×10^3			
-0.2327×10^2	0.6303×10^2	0.1143×10^3	0.3357×10^3		
-0.6827×10^2	-0.1379×10^3	-0.8105×10^2	-0.5034×10^3	0.1538×10^4	
-0.3166×10^2	-0.1301×10^3	-0.2323×10^2	-0.4264×10^3	0.1078×10^4	0.1008×10^4
Phase	me	se	Error (se)	$\tau_l+\rho_l$	
Δ_C	0.839	0.788	0.054	−0.027	
Δ_T	−2.324	−2.206	0.060	0	
Δ_{LS}	0.76	0.71	0.11	0	

TABLE VIII. (*Continued*).

		ϵ_2 fixed at the me value 25.0 MeV			
Groups	N_{obs}	N_{df}	χ^2_{se}		
10	41	35	32.00		
Phase	me	se	Error (se)	$\tau_I+\rho_I$	$\bar{\Delta}_0$
$^1S_0$	48.77	48.87	0.12	−0.04	−0.04
$^3P_0$	8.61	8.65	0.35	−0.03	
$^3P_1$	−4.57	−4.52	0.13	−0.03	
$^3P_2$	2.53	2.52	0.11	−0.03	
$^1D_2$	0.771	0.775	0.039	−0.021	
Δ_C	0.839	0.859	0.051	−0.027	
Δ_T	−2.324	−2.319	0.044	0	
Δ_{LS}	0.76	0.74	0.11	0	

error matrix at the minimum of χ^2 with respect to variations in $\delta(^1S_0)$, $\delta(^3P_0)$, $\delta(^3P_1)$, $\delta(^3P_2)$, $\delta(^1D_2)$, and the ϵ_2 mixing parameter, which does give correctly the dependence of χ^2 on the phase shifts for this cluster.

We have examined the quality of this description of the χ^2 hypersurface by computing χ^2 for the Nijmegen potential[27] [with the electromagnetic potential (Sec. III) added] in two ways: (i) exact—by direct comparison with the data and (ii) with the inverse error matrices of Table VIII. The error matrices gave $\chi^2=666$ ($\chi^2/N_{df}\approx 1.9$), where as the data gave $\chi^2=607$ ($\chi^2/N_{df}\approx 1.8$).

VII. SUMMARY OF CONCLUSIONS

In this analysis the pion-coupling constant can be determined from the low-energy data without model-dependent errors, which is an important improvement over previous analyses. We find $g^2_{pp\pi^0}/4\pi=14.5\pm1.2$, but the inclusion of unpublished data or higher-energy data reduces the value by about one standard deviation (13.4 ± 1.0). A table of multienergy phase shifts is given, which makes it easy to compute the phase shifts at every desired energy between 0 and 30 MeV. With the Foldy corrections listed in the table one can include vacuum polarization and improved Coulomb in nuclear potential models if the $^1S_0$ phase shift of the potential is computed with, for the electromagnetic interaction only, the standard point-Coulomb interaction. Flaws in the Paris[28] and Nijmegen[27] potential are noticed. In order to compare with previous analyses, effective range parameters derived from the multienergy phases are given. The single-energy phase shifts and error matrices, to be used if one adjusts model parameters to the 0–30 MeV pp scattering data, have been tested for the Nijmegen potential to give a χ^2/N_{df} accurate up to 0.1.

ACKNOWLEDGMENTS

We wish to thank Dr. T. Rijken, Drs. W. Derks, and Drs. V. Stoks for many useful discussions. Part of this work was included in the research program of the Stichting voor Fundamenteel Onderzoek der Materie (F.O.M.) with financial support from the Nederlandse Organisatie voor Zuiver-Wetenschappelijk Onderzoek (Z.W.O.).

APPENDIX: HOW NONSTATISTICAL ARE THE DATA?

In this Appendix we want to see how the data spread around the model values. The theoretical framework has already been presented in Sec. V A. The total χ^2 (χ^2_{tot}) is in our case surely compatible with the data being drawn around the model values [Eq. (69)]. Here we want to say more about the distribution of the contributions to χ^2, i.e., the N_{dat} squared terms in Eq. (66). The distribution we find in the me fit we denote by $P_{1,analysis}(\chi^2)$. It is given by

$$P_{1,analysis}(\chi^2)=\frac{1}{N_{dat}}\sum_{i=1}^{N_{dat}}\delta(\chi^2-\chi_i^2)\ . \tag{A1}$$

This distribution has to be compared with the theoretical probability distribution function, the χ^2 distribution for 1 degree of freedom $P_1(\chi^2)$ of Eq. (68). This comparison is made in a histogram in Fig. 8, but it is difficult to judge the agreement between the distributions from such a figure. We believe it is better to give the moments of the distributions, because errors can be given for these moments. The moments μ'_n of a distribution $P(t)$ [with $0\le t<\infty$] are given by

$$\mu'_n=\int_0^\infty dt\ P(t)t^n\ , \tag{A2}$$

and the central moments μ_n are given by

$$\mu_n=\int_0^\infty dt\ P(t)(t-\mu'_1)^n\ . \tag{A3}$$

The error in μ'_n from a draw of N out of $P(t)$ can then be evaluated as

$$\sigma_{\mu'_n}=\left[\frac{\mu'_{2n}-(\mu'_n)^2}{N}\right]^{1/2}\ , \tag{A4}$$

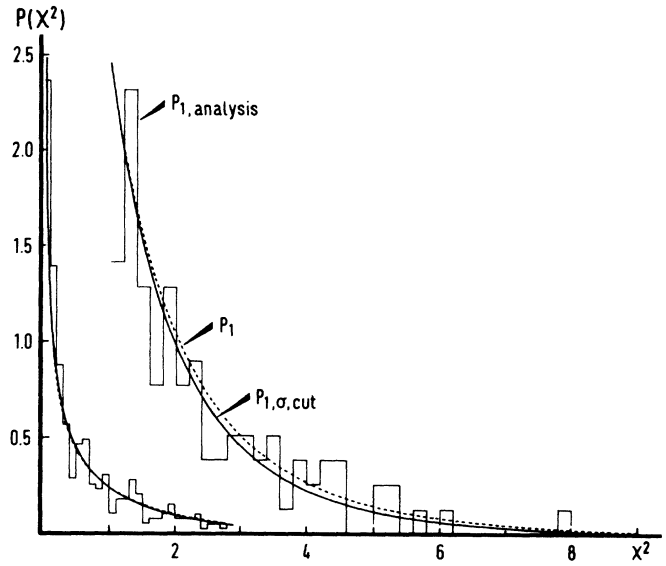

FIG. 8. Probability distribution functions vs χ^2. The tail is enlarged by a factor of 10. The histogram, of 389 data points, represents the experimental distribution in bins $\Delta\chi^2=0.1$ (and $\Delta\chi^2=0.2$ for the tail). — — —: $P_1(\chi^2)$, χ^2 probability distribution function for 1 degree of freedom. ——: $P_{1,\sigma,\text{cut}}(\chi^2)$, χ^2 probability distribution function if we take into account that $\langle\chi^2\rangle=\frac{343}{389}$ and that data points with $\chi^2>9$ have been rejected.

and analogously for σ_{μ_n}.

There are two flaws in $P_1(\chi^2)$ as a comparison for $P_{1,\text{analysis}}(\chi^2)$. First of all, as discussed in Sec. V A,

$$\int_0^\infty dt\, P_{1,\text{analysis}}(t)t=\chi^2_{\text{tot}}/N_{\text{dat}}\ , \tag{A5}$$

where as

$$\int_0^\infty dt\, P_1(t)t=1\ . \tag{A6}$$

The expectation value $\langle\chi^2_{\text{tot}}\rangle=N_{\text{df}}=343$, but $N_{\text{dat}}=389$, because the normalizations (17 overall norms plus 12 angle-dependent normalization factors) contribute to χ^2, we use 12 model parameters, and there are five unnormed groups of data. Therefore, a better probability distribution function to compare $P_{1,\text{analysis}}(\chi^2)$ with is the somewhat narrowed probability distribution function of Eq. (71) with $\alpha=\frac{343}{389}$. Second, we have rejected all data with $\chi_i^2>9$, which influences of course primarily the higher moments. Therefore, we believe it is best to compare the moments of $P_{1,\text{analysis}}(\chi^2)$ with those of

$$P_{1,\sigma,\text{cut}}(\chi^2)=[\sigma\sqrt{2}\gamma(\tfrac{1}{2},\tfrac{9}{2}\sigma^{-2})]^{-1}\times e^{-\chi^2/2\sigma^2}(\chi^2)^{-1/2}\theta(9-\chi^2)\ , \tag{A7}$$

with $\gamma(\alpha,z)$ the incomplete gamma function and σ chosen in order to have $\langle\chi^2\rangle=\frac{343}{389}$, thus $\sigma=0.89677$. This $P_{1,\sigma,\text{cut}}(\chi^2)$ still has a flaw as a comparison probability distribution function for $P_{1,\text{analysis}}(\chi^2)$, since measurements of different groups are treated in the same way.

TABLE IX. Moments μ'_n and central moments μ_n for our analysis of the data and the moments of two comparison probability distribution functions. Errors are given for a draw of 389 points. In the moments given for our analysis, contributions of normalization data are included. For definitions, see the Appendix.

	$P_1(\chi^2)$	$P_{1,\sigma,\text{cut}}(\chi^2)$	$P_{1,\text{analysis}}(\chi^2)$
μ'_1	1.000±0.072	0.882±0.061	0.883
μ'_2	3.000±0.050	2.24±0.32	2.24
μ'_3	15.0±5.1	8.8±2.0	8.5
μ'_4	105±72	44±14	40
μ_2	2.00±0.38	1.46±0.23	1.46
μ_3	8.0±3.9	4.3±1.3	3.9
μ_4	60±55	21.9±8.7	18.3

The lower moments of $P_1(\chi^2)$, $P_{1,\sigma,\text{cut}}(\chi^2)$, and $P_{1,\text{analysis}}(\chi^2)$ are given in Table IX together with their errors. All of the four lower moments of $P_{1,\text{analysis}}(\chi^2)$ agree (almost too good) with those of $P_{1,\sigma,\text{cut}}(\chi^2)$, so the distribution of the contributions to χ^2 is very near to what one would expect for statistical data. In the histogram (Fig. 8) where the above probability distribution functions are displayed, one can see that to the eye both probability distribution functions agree with the experimental distribution $P_{1,\text{analysis}}(\chi^2)$.

[1]J. P. Naisse, Report No. ulb/ph/TH-8, Université Libre de Bruxelles, 1976 (unpublished).
[2]J. P. Naisse, Nucl. Phys. **A278**, 506 (1977).
[3]Ch. Thomann, J. E. Benn, and S. Münch, Nucl. Phys. **A303**, 457 (1978).
[4]H. Wassmer and H. Mühry, Helv. Phys. Acta **46**, 626 (1973).
[5]J. Birchall, E. Baumgartner, H. M. Friess, H. Mühry, F. Rösel, and D. Trautman, Helv. Phys. Acta **50**, 509 (1977).
[6]M. D. Barker, P. C. Colby, W. Haeberli, and P. Signell, Phys. Rev. Lett. **48**, 918 (1982).
[7]M. D. Barker, P. C. Colby, W. Haeberli, and P. Signell, Phys. Rev. Lett. **49**, 1056 (1982).
[8]N. Jarmie and J. H. Jett, Phys. Rev. C **13**, 2554 (1976).
[9]G. Bittner and W. Kretschmer, Phys. Rev. Lett. **43**, 330 (1979).
[10]H. Obermeyer, H. Kuiper, B. Seidler, and K. Frank, Nucl. Phys. **A344**, 75 (1980).
[11]H. P. Noyes and H. M. Lipinski, Phys. Rev. C **4**, 995 (1971).
[12]M. S. Sher, P. Signell, and L. Heller, Ann. Phys. (N.Y.) **58**, 1 (1970).
[13]G. J. M. Austen and J. J. de Swart, Phys. Rev. Lett. **50**, 2039 (1983).
[14]J. J. de Swart, J. R. M. Bergervoet, P. C. M. van Campen, and W. A. M. van der Sanden, in *Advanced Methods in the Evaluation of Nuclear Scattering Data*, Vol. 236 of *Lecture Notes in*

Physics, edited by H. J. Krappe and R. Lipperheide (Springer-Verlag, Berlin, 1985), p. 179.
[15]M. Gursky and L. Heller, Phys. Rev. **136**, B1693 (1964).
[16]H. P. Noyes, Annu. Rev. Nucl. Sci. **22**, 465 (1972).
[17]W. A. van der Sanden, A. H. Emmen, and J. J. de Swart, Report No. THEF-NYM-83.11, Nijmegen, 1983 (unpublished).
[18]L. Mathelitsch and B. J. VerWest, Phys. Rev. C **29**, 739 (1984).
[19]L. Heller, Phys. Rev. **120**, 627 (1960).
[20]M. Cini, S. Fubini, and A. Stanghellini, Phys. Rev. **114**, 1633 (1959).
[21]D. Y. Wong and H. P. Noyes, Phys. Rev. **126**, 1866 (1962).
[22]R. L. Jaffe and F. E. Low, Phys. Rev. D **19**, 2105 (1979).
[23]Y. A. Simonov, Phys. Lett. **107B**, 1 (1981).
[24]P. J. Mulders, Phys. Rev. D **28**, 443 (1983).
[25]H. Feshbach and E. L. Lomon, Ann. Phys. (N.Y.) **29**, 19 (1964).
[26]L. Durand III, Phys. Rev. **108**, 1597 (1957).
[27]M. M. Nagels, T. A. Rijken, and J. J. de Swart, Phys. Rev. D **17**, 768 (1978).
[28]M. Lacombe, B. Loiseau, J. M. Richard, R. Vinh Mau, J. Côté, P. Pirès, and R. de Tourreil, Phys. Rev. C **21**, 861 (1980).
[29]P. M. Hegland, Ph.D. thesis, University of Minnesota, 1976.
[30]P. M. Hegland, R. E. Brown, J. S. Lilley, and J. A. Koepke, Phys. Rev. Lett. **39**, 9 (1977).
[31]P. A. Lovoi, Ph.D. thesis, University of California, Los Alamos, 1975.
[32]P. A. Lovoi, G. G. Ohlsen, N. Jarmie, C. E. Moss, and D. M. Stupin, in *Proceedings of the Fourth International Symposium on Polarization Phenomena in Nuclear Reactions, Zürich, August, 1975,* edited by W. Grüebler and V. König (Birkhäuser Verlag, Basel, 1976), p. 450.
[33]J. Arvieux, R. Darves-Blanc, J. L. Durand, A. Fiore, L. Van Sen, and C. Perrin, in Proceedings of the Third International Symposium, Madison, Wisconsin, 1970 (unpublished), p. 435.
[34]R. A. Arndt, R. H. Hackman, and L. D. Roper, Phys. Rev. C **9**, 555 (1974).
[35]R. A. Arndt, R. H. Hackman, and L. D. Roper, Phys. Rev. C **15**, 1002 (1977).
[36]R. A. Arndt, L. D. Roper, R. A. Bryan, R. C. Clark, B. J. VerWest, and P. Signell, Phys. Rev. D **28**, 97 (1983).
[37]R. A. Arndt, J. S. Hyslop III, and L. D. Roper, Phys. Rev. D **35**, 128 (1987).
[38]J. Bystricky, C. Lechanoine, and F. Lehar, Saclay Report No. D.Ph.P.E. 79-01, 1979 (unpublished).
[39]J. Bystricky, C. Lechanoine-Leluc, and F. Lehar, J. Phys. (Paris) **48**, 199 (1987).
[40]G. E. Bohannon, T. Burt, and P. Signell, Phys. Rev. C **13**, 1816 (1976).
[41]A. A. Logunov and A. N. Tavkhelidze, Nuovo Cimento **29**, 380 (1963).
[42]R. Blankenbecler and R. Sugar, Phys. Rev. **142**, 1051 (1966).
[43]V. G. Kadyshevsky, Nucl. Phys. **B6**, 125 (1968).
[44]V. G. Kadyshevsky, Nuovo Cimento **55**, 275 (1968).
[45]M. H. Partovi and E. L. Lomon, Phys. Rev. D **2**, 1999 (1970).
[46]K. Erkelenz, Phys. Rep. C **13**, 191 (1974).
[47]J. J. de Swart and M. M. Nagels, Fortschr. Phys. **26**, 215 (1978).
[48]G. Breit, E. U. Condon, and R. A. Present, Phys. Rev. **50**, 825 (1936).
[49]L. Landau and J. Smorodinsky, J. Phys. USSR **8**, 154 (1944).
[50]J. Blatt, Phys. Rev. **74**, 92 (1948).
[51]H. Bethe, Phys. Rev. **76**, 38 (1949).
[52]G. J. M. Austen, Ph.D. thesis, University of Nijmegen, 1982.
[53]H. van Haeringen and L. P. Kok, Phys. Rev. **26**, 1218 (1982).
[54]G. Breit, Phys. Rev. **99**, 1581 (1955).
[55]W. A. van der Sanden (unpublished).
[56]M. H. Ross and G. Shaw, Ann. Phys. (N.Y.) **13**, 147 (1961).
[57]J. J. de Swart and C. Dullemond, Ann. Phys. (N.Y.) **19**, 458 (1962).
[58]E. A. Uehling, Phys. Rev. **48**, 55 (1935).
[59]L. D. Knutson and D. Chiang, Phys. Rev. C **18**, 1958 (1978).
[60]*Handbook of Mathematical Functions,* edited by M. Abramowitz and I. A. Stegun (Dover, New York, 1970).
[61]H. P. Stapp, T. J. Ypsilantis, and N. Metropolis, Phys. Rev. **105**, 302 (1957).
[62]J. R. Taylor, Nuovo Cimento **23B**, 313 (1974).
[63]J. R. Taylor, Nuovo Cimento **26A**, 48 (1975).
[64]M. H. MacGregor, M. J. Moravcsik, and H. P. Stapp, Annu. Rev. Nucl. Sci. **10**, 291 (1960).
[65]N. Hoshizaki, Prog. Theor. Phys. Suppl. **42**, 107 (1968).
[66]L. L. Foldy and E. Eriksen, Phys. Rev. **98**, 775 (1955).
[67]W. M. Derks, W. A. van der Sanden, and J. J. de Swart (unpublished).
[68]R. J. Slobodrian, H. E. Conzett, E. Shield, and W. Tivol, Phys. Rev. **174**, 1122 (1968).
[69]D. J. Knecht, P. F. Dahl, and S. Messelt, Phys. Rev. **148**, 1031 (1966).
[70]J. E. Brolley, J. D. Seagrave, and J. G. Beery, Phys. Rev. **135**, B1119 (1964).
[71]J. D. Hutton, W. Haeberli, L. D. Knutson, and P. Signell, Phys. Rev. Lett. **35**, 429 (1975).
[72]J. Bystricky and F. Lehar, *Nucleon-Nucleon Scattering Data,* Physics Data 11-1 (Fachinformationszentrum, Karlsruhe, Federal Republic of Germany, 1978).
[73]J. Bystricky and F. Lehar, *Nucleon-Nucleon Scattering Data,* Physics Data 11-3 (Fachinformationszentrum, Karlsruhe, Federal Republic of Germany, 1981).
[74]W. Kretschmer, M. Haller, A. Rauscher, R. Schmitt, W. Schuster, W. Grüebler, C. Forstner, V. König, and P. A. Schmelzbach, in Book of Contributions, Eleventh International IUPAP Conference on Few Body Systems in Particle and Nuclear Physics, Tokyo and Sendai, 1986, edited by T. Sasakawa, K. Nisimura, S. Oryu, and S. Ishikawa (unpublished).
[75]K. Imai, K. Nisimura, N. Tamura, and A. Sato, Nucl. Phys. **A246**, 76 (1975).
[76]R. J. Slobodrian, J. S. McKee, H. Bichsel, and W. F. Tivol, Phys. Rev. Lett. **19**, 704 (1967).
[77]L. H. Johnston and D. E. Young, Phys. Rev. **116**, 989 (1959).
[78]N. Jarmie, J. H. Jett, J. L. Detch, Jr., and R. L. Hutson, Phys. Rev. Lett. **25**, 34 (1970).
[79]N. Jarmie, R. E. Brown, R. L. Hutson, and J. L. Detch, Jr., Phys. Rev. Lett. **24**, 240 (1970).
[80]P. Catillon, M. Chapellier, and D. Garreta, Nucl. Phys. **B2**, 93 (1967).
[81]S. Kikuchi, J. Sanada, S. Suwa, I. Hayashi, K. Nisimura, and K. Fukunaga, J. Phys. Soc. Jpn. **15**, 9 (1960).
[82]W. A. Blanpied, Phys. Rev. **116**, 738 (1959).
[83]J. L. Yntema and M. G. White, Phys. Rev. **95**, 1226 (1954).
[84]P. Catillon, J. Sura, and A. Tarrats, Phys. Rev. Lett. **20**, 602 (1968).
[85]C. J. Batty, G. H. Stafford, and R. S. Gilmore, Nucl. Phys. **51**, 225 (1964).
[86]T. H. Jeong, L. H. Johnston, and D. E. Young, Phys. Rev. **118**, 1080 (1960).
[87]D. Garreta, K. Nisimura, and M. Fruneau, Phys. Lett. **31B**,

363 (1970).
[88]N. Jarmie, J. E. Brolley, H. Kruse, H. C. Bryant, and R. Smythe, Phys. Rev. **155**, 1438 (1967).
[89]P. Christmas and A. E. Taylor, Nucl. Phys. **41**, 388 (1963).
[90]A. Ashmore, B. W. Davies, H. Devine, S. J. Hoey, J. Litt, H. E. Shepherd, R. C. Hanna, and H. E. Robertson, Nucl. Phys. **73**, 256 (1965).
[91]L. H. Johnston and Yung Su Tsai, Phys. Rev. **115**, 1293 (1959).
[92]C. J. Batty, R. S. Gilmore, and G. H. Stafford, Nucl. Phys. **45**, 481 (1963).
[93]O. N. Jarvis and B. Rose, Phys. Lett. **15**, 271 (1965).
[94]J. Holdeman, P. Signell, and M. Sher, Phys. Rev. Lett. **24**, 243 (1970).
[95]O. Dumbrajs, R. Koch, H. Pilkuhn, G. C. Oades, H. Behrens, J. J. de Swart, and P. Kroll, Nucl. Phys. **B216**, 277 (1983).
[96]J. R. Bergervoet, P. C. van Campen, T. A. Rijken, and J. J. de Swart, Phys. Rev. Lett. **59**, 2255 (1987).
[97]T. Obinata and M. Wada, Prog. Theor. Phys. **53**, 732 (1975).
[98]T. Obinata and M. Wada, Prog. Theor. Phys. **57**, 1984 (1977).
[99]T. Obinata and M. Wada, Prog. Theor. Phys. **61**, 1697 (1979).
[100]K. Holinde and R. Machleidt, Nucl. Phys. **A247**, 495 (1975).
[101]K. Holinde and R. Machleidt, Nucl. Phys. **A256**, 479 (1976).
[102]K. Holinde and R. Machleidt, Nucl. Phys. **A280**, 429 (1977).
[103]R. B. Wiringa, R. A. Smith, and T. L. Ainsworth, Phys. Rev. C **29**, 1207 (1984).
[104]G. Piepke, Helv. Phys. Acta **58**, 1049 (1985).
[105]J. J. de Swart, W. A. van der Sanden, and W. M. Derks, Nucl. Phys. **A416**, 299c (1984).